University POLITEHNICA of Bucharest

Doctoral School of Electrical Engineering Faculty

Ph.D. THESIS - Summary

Energy consumption optimization strategies for electric vehicles

Doctoral Supervisor:

Prof. Dr. Ing. Aurelian CRĂCIUNESCU

Author:

Ing. Cristian-Liviu POPESCU

BUCHAREST

2023

CONTENTS

I. INTRODUCTION TO THE RESEARCH SUBJECT

I.1. Main pursued problems

In preparation of research objective, preliminary studies have been performed. Electric cars main sizes related to electrification and main characteristics of principal types of motors that could be used for electric traction are presented in next two tables.

Table I-1. Increasing sizes of main characteristics related to electrification

Electric Mobility	**Total Weight**	**Speed**	**Range**	**Electric Powertrain**	**Battery**
Micromobility*	<1/4 t	25 km/h	30 km	250 W	280Wh
Two / Three wheelers					
Low speed electric vehicles		40-70 km/h			
Light-commercial electric vehicles					
Passenger cars		200-250 km/h	500 km	100-500 kW	100 kWh
Busses			500 km		660 kWh
Trucks					

Table I-2. Main characteristics of principal types of motors analyzed in preparation for the actual research

Characteristics	**Motor type**			
	DC	Induction Motor	Permanent Magnets	Switched Reluctance Motor
Power density	Low	Medium	Very high	Medium
Efficiency	Low	Medium	Very high	Medium
Controllability	Very high	Very high	High	Medium
Reliability	Medium	Very high	High	Very high
Technological maturity	Very high	Very high	High	High
Cost	Low	Very low	High	Low

Another advantage of electric motors is also emphasized by the possibility to integrate multiple motors in a vehicle powertrain.

I.2. Research objective

The main objective is to develop energy consumption optimization strategies for EV using high-power density electric motors, and more precisely permanent magnets motors completed by the usage of multi-motor powertrains. Specific attention is dedicated to modelling and simulation of electric vehicles, with specific focus to the powertrain, and effectively how a vehicle request is transformed into operating points for the powertrain, and powertrain characteristics. The next sub-objective concerns multi-motor powertrain research to determine the main strategies for motor torque allocation methods, criteria for energy efficiency optimization, and the study of the powertrain limits depending on vehicle characteristics. Regarding electric motors, there is research for improving control of BLDC motors with advanced methods to enhance motor capabilities (speed, torque, yield) and vehicle energy efficiency. Another aspect proposed to be explored concerns multi-motor performant powertrains by the choice of motors and methodologies to investigate and construct the efficiency maps. For experimental verification there is an interest in developing multi-motor platforms integrating specific motor controllers and a dedicated supervision system.

II. ELECTRIC VEHICLES: MODELING AND SIMULATION. POWERTRAIN REQUEST CALCULATION

II.1. Realization of the models for multi-motor powertrains

Method for torque and power calculation in powertrains using multiple motors

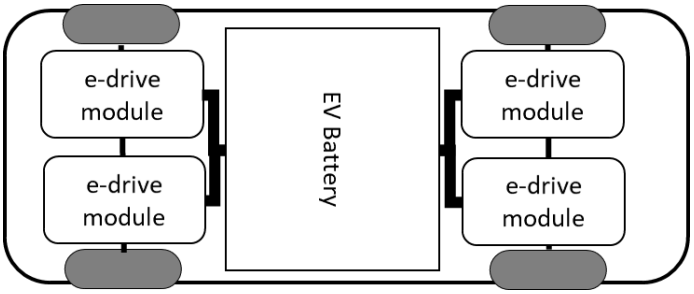

Fig. II-1. Vehicle in multi-motor configuration: four-motor solution

It is possible to calculate the torque and power for each motor, covering all situations, from one-motor powertrain to multiple motor-powertrain (*m* motors). The method is presented in the long version of the thesis. For example, a solution with two PM motors is implemented under simulation. Each axle is covered by one motor and the total torque is distributed between the front and rear axle.

II.2. Simulation

Principally, a general view can be represented as shown in Fig. II-2., by three main modules covering: requests, systems control, and mechanical power generation.

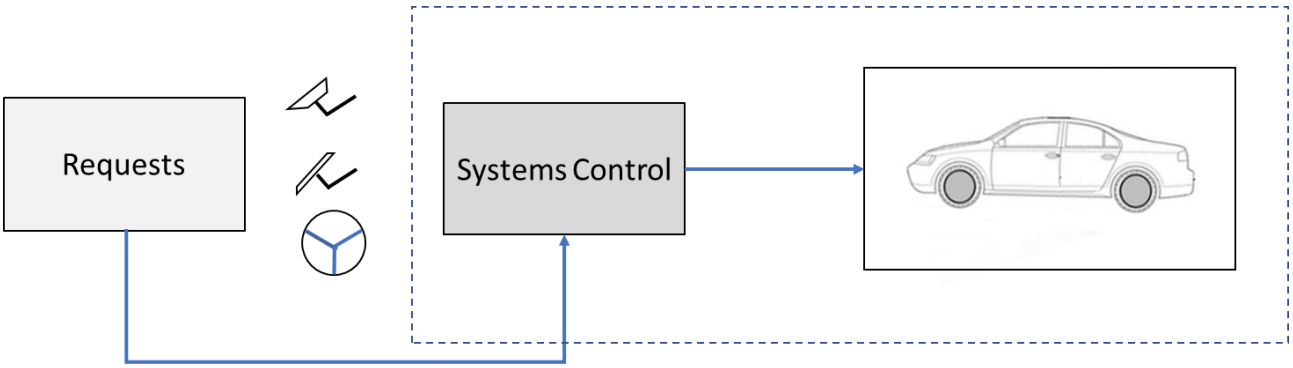

Fig. II-2. Vehicle simulation - general view on modules

The requests are generated by a driving cycle velocity profile. The information is transformed by a driver model in acceleration, deceleration/braking requests. The systems control module integrates models dedicated to onboard energy management and the control of the powertrain. The generation of the mechanical power and the drivetrain models are behind the vehicle box.

II.3. Results Obtained Involving Multiple Motors in an EV Powertrain

II.3.1. Method to pass from a testing cycle data to torque requirement

Table II-1. Characteristics of the vehicle for torque requirement study

Characteristic	Value	Measurement Unit
Maximum mass	250	Kg
Wheel radius	0.275	M
Aerodynamic drag coefficient	0.46	-
Frontal area	0.92	m^2
Transmission ratio motor to wheel	1	-

Table II-2. Resistant forces coefficients for torque requirement study

Characteristic	Value
Tractive effort coefficient	0.8
Rolling resistance coefficient	0.013

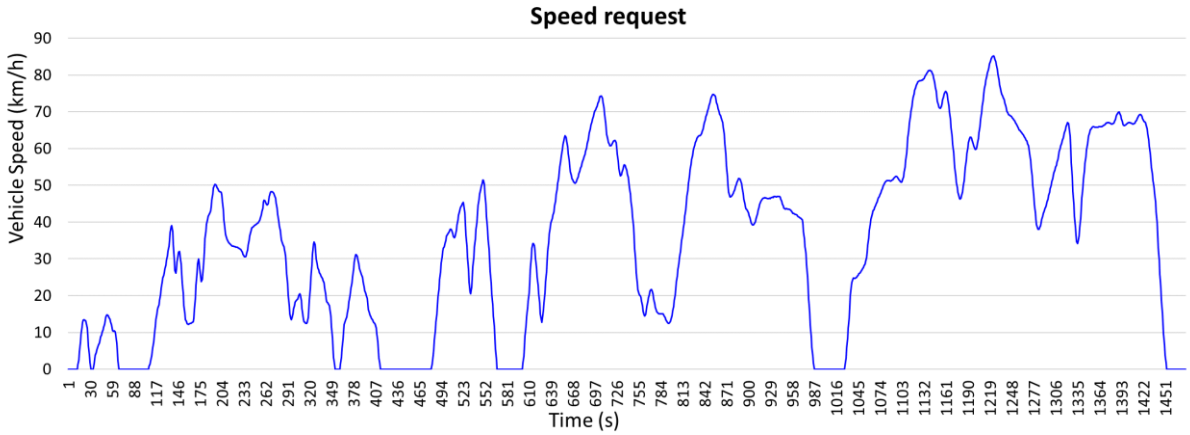

Fig. II-3. WLTC – class 2 – speed evolution

From the speed profile results the acceleration request.

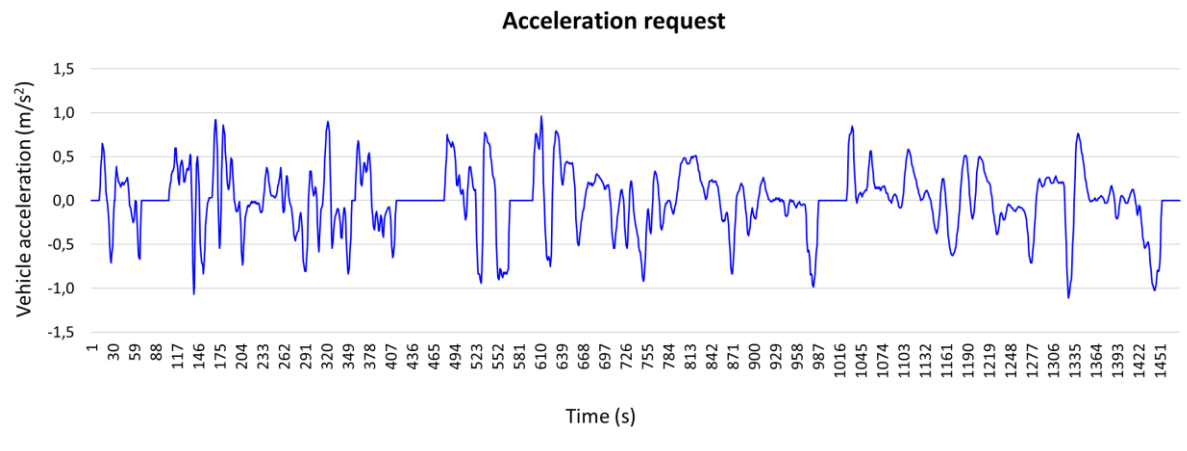

Fig. II-4. WLTC – class 2 – acceleration evolution for torque requirement study

For moving the vehicle with an acceleration a, the tractive effort is

$$F_t = F_{ra} + G_t + F_f + Ma, \tag{II-1}$$

where F_{ra} is the aerodynamic drag, G_t the grading resistance, F_f the rolling resistance, M the mass of the vehicle, and a the acceleration.

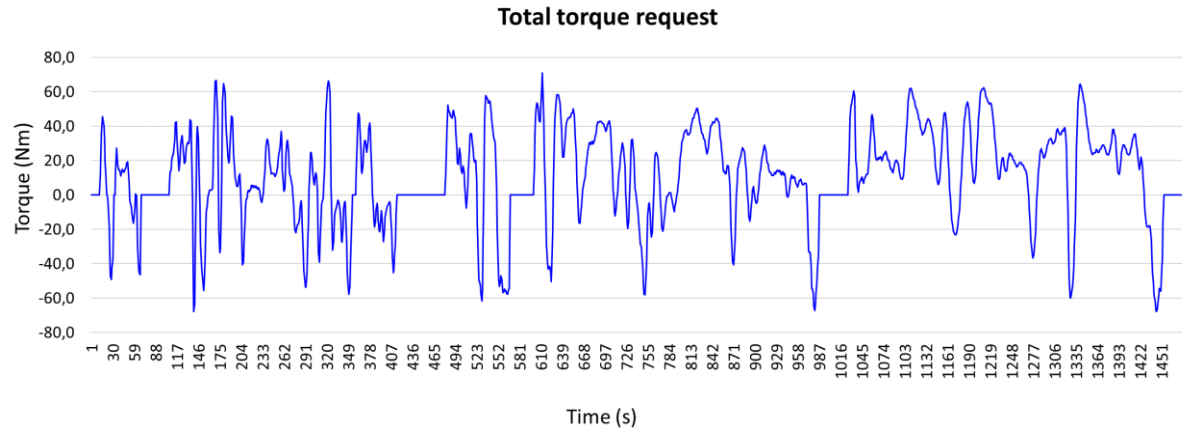

Fig. II-5. Evolution of the total torque request at wheels level

The situation when the vehicle is running on a flat surface, $G_t = 0$. For each wheel, the normal force on the wheel multiplied by the tractive effort coefficient gives the maximum force that the respective wheel can provide keeping the adherence. In our case all wheels contribute to the tractive effort generation, so the total torque request represents the sum of torques at each motor shaft, neglecting the mechanical losses in the transmissions. The resulted torque is the product between the wheel radius and the tractive effort, Fig. II-5.

II.3.2. Operational area coverage by the powertrain

Building the operating points for the powertrain

The requests for speed (Fig. II-3.) and total torque (Fig. II-5.) are functions of time. Substituting the time between the two functions is possible to represent the torque requests as a function of speed. Using discrete data, the dependence between the powertrain torque request and speed request is a point cloud as shown in the next figure. Further, the point cloud is called **operating points**.

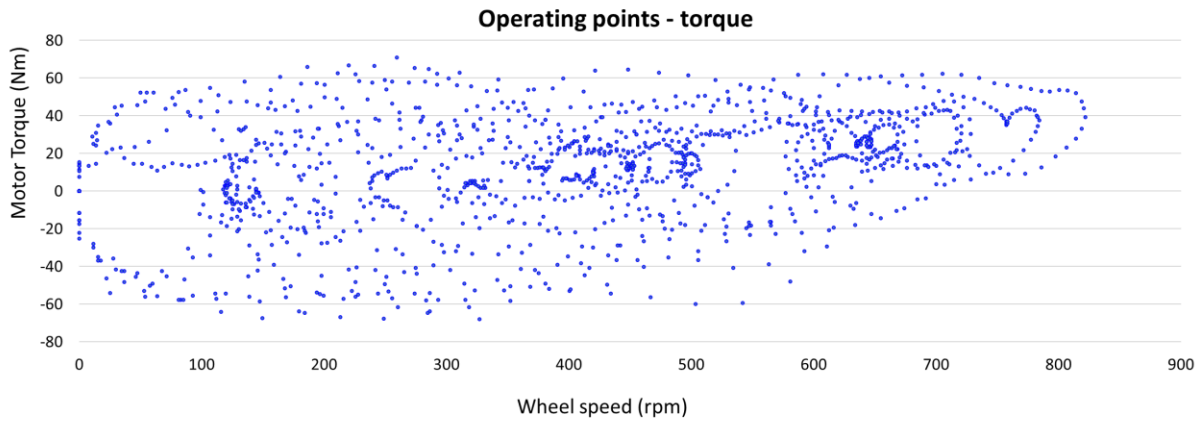

Fig. II-6. Operating points requirement for the powertrain – torque

Characteristics of the motors used in the investigation

Two BLDC motors are integrated as an example for powertrain coverage.

Table II-3. Characteristics of the motors for torque requirement study

Characteristics	Motor One	Motor Two
Nominal / Max Power	4 / 8 kW	3 / 6 kW
Torque constant	1.655 Nm/A	1.800 Nm/A
Internal resistance	0.128 Ω	0.130 Ω
Maximum torque	182 Nm	180 Nm
Maximum speed	880 rpm	880 rpm

The process using analytic calculation by programming to obtain the motor characteristics is presented in Fig. II-7. The curve of the maximum power is obtained for an operating voltage of 72V.

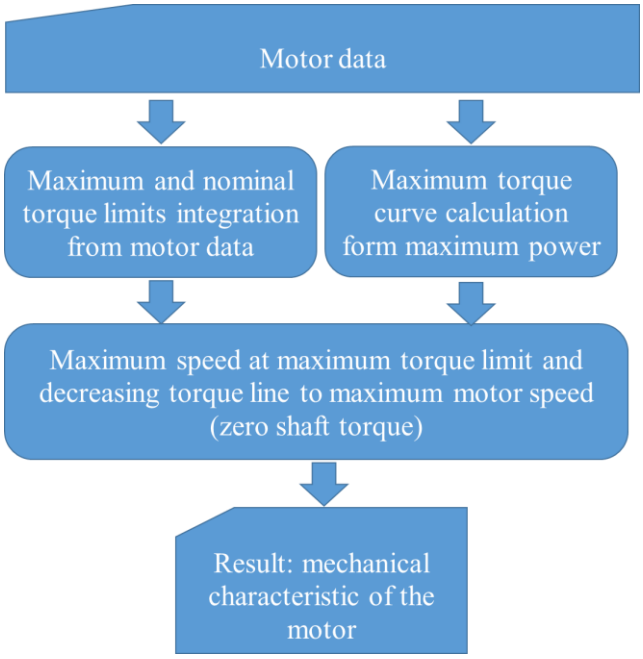

Fig. II-7. Mechanical characteristic determination process for operational area study

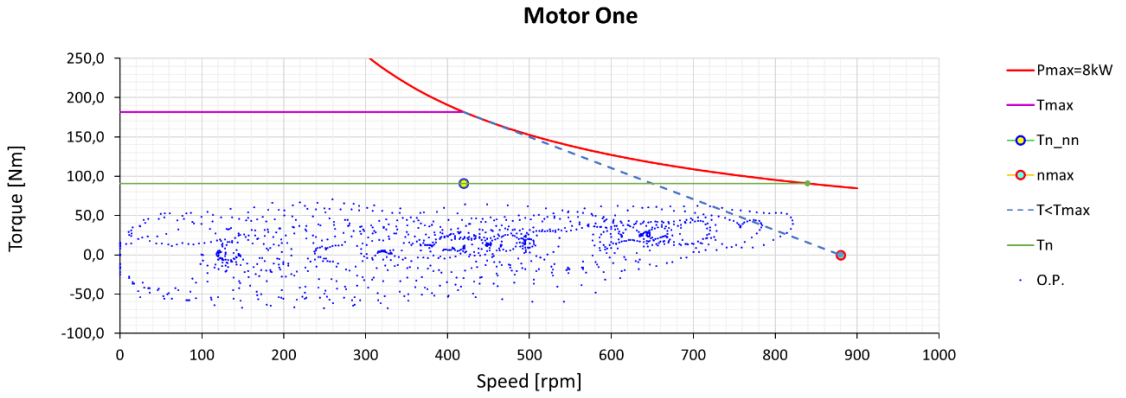

Fig. II-8. Operating points and mechanical characteristic of Motor One

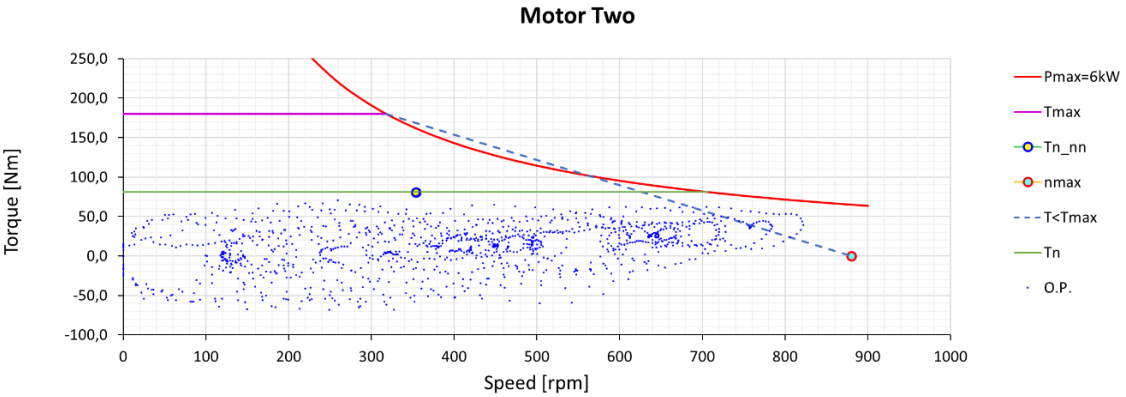

Fig. II-9. Operating points and mechanical characteristic of Motor Two

II.4. Conclusion

For the two investigated motors, each motor can cover the vehicle request, under nominal values for almost all the operational area. Specific research can be performed for high-speed behavior, when the nominal power is exceeded. It concerns the capabilities of each motor to cover the powertrain needs and the response for an additional grading resistance. This investigation is realized in the second part of the chapter III.

III. Optimizations Based on Load Allocation between Motors and Powertrain Limits

The present chapter analyses multi-motor solutions by searching energy efficiency using load distribution methods between motors.

III.1. Static load allocation methods

Preserving the vehicle stability, a static load allocation scenario can be defined as a charge repartition fixed algorithm between the powertrain motors applied in each operating point. The repartition algorithm doesn't change when passing from an operating point to another. In this case, there is no need to make additional calculations for each operating point of the powertrain.

III.1.1. Definitions: complementary, percentual, proportional and optimal load distributions

A possibility is to imply the motors one by one up to a certain torque level. When the requested torque exceeds this level, the motor in use remains at the same torque, and the complementary torque request is covered by another motor. This allocation method can be called a **complementary load distribution**. When the motors of the powertrains are involved simultaneously, all the time, by allocating a fixed percentage of the torque request to each motor, this torque allocation can be called a **percentual load distribution**. The maximum power of the multi-motor-powertrain is the sum of the maximum power of each motor. When the percentage of the torque allocation for one motor is calculated as a rapport between the maximum power of the motor and the maximum power of the powertrain, the torque allocation can be called a **proportional load distribution**. The case when the percentage of the torque allocation for each motor is determined as a result of the efficiency optimization of the powertrain, and the respective torque allocation between motors produces any time the highest efficiency than any other percentual torque allocation the allocation method can be called an **optimal load distribution**.

III.1.2. Complementary load distribution

The vehicle simulation presented in section II.2 is considered to exemplify the complementary load distribution results. The vehicle model used is for a classic one (limousine) offering two-wheel and four-wheel driving capabilities, with two IPMSM (Internal Permanent Magnets Synchronous Motor).

Table III-1. Characteristics of the vehicle for studying complementary load distribution

Characteristic	Value	Measurement Unit
Vehicle mass	1200	kg
Wheel radius	0.3	m
Aerodynamic drag coefficient	0.3	-
Frontal area	2	m^2
Transmission rapport motor to wheel	6.8	-

Table III-2. Resistant forces coefficients for complementary load distribution study

Characteristic	Value
Tractive effort coefficient	0.9
Rolling resistant coefficient	0.007

Fig. III-1. FTP75 speed request

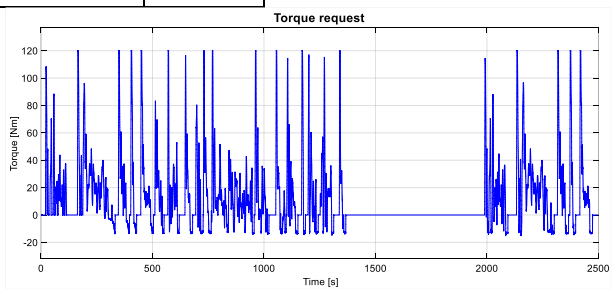

Fig. III-2. Total torque request for complementary load distribution study

Observing this request, instead of using a single motor to realize the vehicle's powertrain, it is possible to distribute the total torque (maximum 120 Nm) between two electric smaller motors: a first one covering a low torque region (40 Nm), and the second completing the additional torque necessary to answer the request for higher torque (80 Nm). The electrical machines are named in this situation Motor 1 and Motor 2, for difference than the precedent examples with the two BLDC motors.

Applying the complementary load allocation, Motor 2 starts first covering a maximum torque of 80 Nm. When the torque request exceeds the capabilities of Motor 2, Motor 1 covers the difference with a maximum torque of 40 Nm. It is also possible to use the smallest motor, as a principal one with a coverage of a maximum torque of 40 Nm, and complete by Motor 2 when the capabilities of Motor 1 are exceeded.

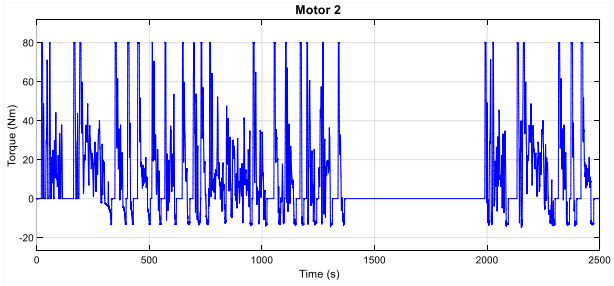

Fig. III-3. Complementary load distribution - load for Motor 2, Motor 2 starts first

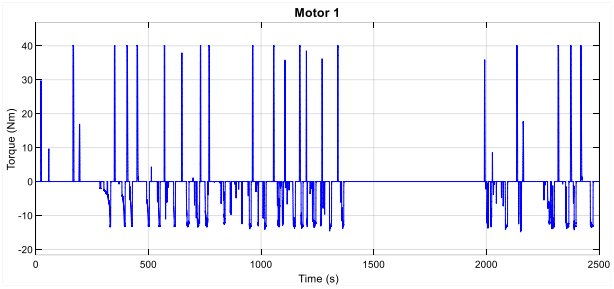

Fig. III-4. Complementary load distribution - load for Motor 1, Motor 2 starts first

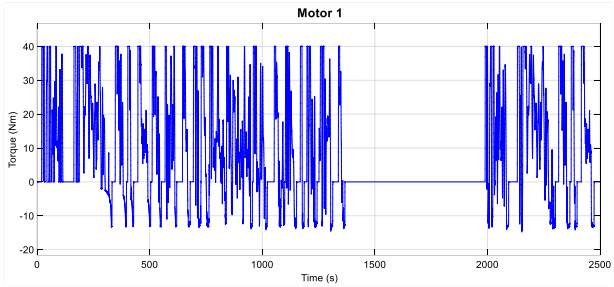

Fig. III-5. Complementary load distribution - load for Motor 1, Motor 1 starts firs

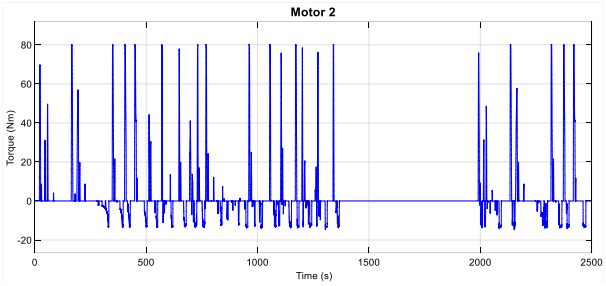

Fig. III-6. Complementary load distribution - load for Motor 2, Motor 1 starts first

The analysis of electric energy used during the driving cycle FTP75 follows the battery SOC.

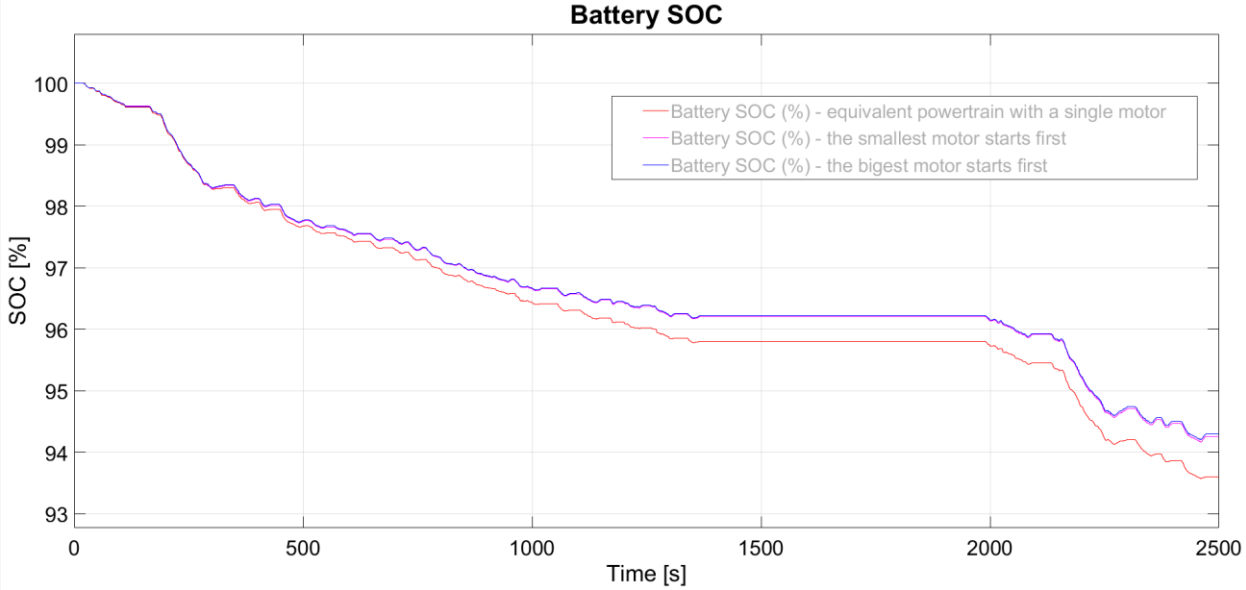

Fig. III-7. Complementary load distribution - state of charge evolution

Conclusion

For this example, the equivalent powertrain with a single motor would consume more energy than the solution with two motors using a complementary load distribution (about 10% more). The order

of which the motors are involved is not without importance and can generate more energy efficiency (in the simulation, about 1% more).

III.1.3. Load distributions using a fixed percentage: percentual, proportional and optimal load distributions

Percentual load distribution

All motors participate simultaneously in the torque production for any torque level. The rapport between the torque T_m produced by the motor *m*, and the total torque of the powertrain, T_t, is a constant value, the load distribution percentage or coefficient,

$$\lambda_m = \frac{T_m}{T_t}. \tag{III-1}$$

Proportional load distribution

It is a particular case of the percentual load distribution. The load coefficient for the motor *m* is

$$\lambda_m = \frac{P_{Max_m}}{P_{tMax}}. \tag{III-2}$$

where, P_{Max_m} is the maximum mechanical power at the shaft of motor *m*, and P_{tMax} the maximum power of the powertrain.

Optimal load distribution

For an optimal load distribution, it is searched the set of λ_m maximizing the efficiency of the powertrain. To exemplify, two motors with a load distribution coefficient λ_1, and λ_2 are considered. Let $\lambda_1 = \lambda$. The motors are running at same speed $\Omega_1 = \Omega_2 = \Omega$.The efficiency of the powertrain is

$$\eta = \frac{P_{t_1} + P_{t_2}}{P_{t_1} + P_{t_2} + P_{l_1} + P_{l_2}} \tag{III-3}$$

where $P_{t_{1,2}}$ is the mechanical power provided by each motor, and $P_{l_{1,2}}$ the losses of each motor (being represented by Joule losses and iron losses): The efficiency of the powertrain is

$$\eta(\lambda, T, \Omega) = \frac{\lambda T\Omega + (1-\lambda)T\Omega}{T\Omega + R_1\left(\frac{\lambda T}{k_{T_1}}\right)^2 + R_2\left(\frac{(1-\lambda)T}{k_{T_2}}\right)^2 + K_{F_1}\Omega^2 + K_{H_1}\Omega + K_{F_2}\Omega^2 + K_{F_2}\Omega}. \tag{III-4}$$

where $k_{T_{1,2}}$ is the torque constant of each motor, $K_{F_{1,2}}$, $K_{H_{1,2}}$ are the eddy currents losses coefficients, and hysteresis losses coefficients, and $R_{1,2}$ the internal electrical resistance of each motor. It results:

$$\frac{\partial\eta(\lambda, T, \Omega)}{\partial\lambda} = 0 \Rightarrow \lambda = \frac{R_2 k_{T_1}^2}{R_1 k_{T_2}^2 + R_2 k_{T_1}^2}, \tag{III-5}$$

The optimal load distribution coefficient is a constant value for the powertrain depending on internal electric resistance and torque constants of the motors.

Results obtained with load distributions using a fixed percentage

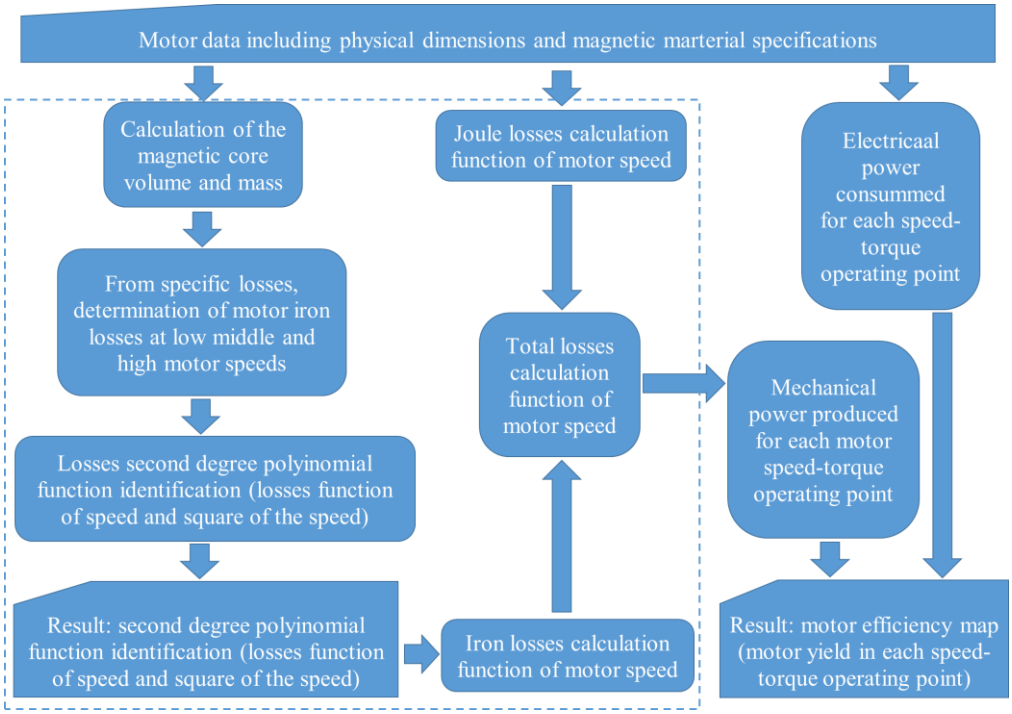

Fig. III-8. Process for determination of motor efficiency maps by analytic calculation

To exemplify the results of load distributions using a fixed percentage, the motors from Table II-3 are considered. The process implemented to determine the efficiency maps is presented in Fig. III-8. Knowing how to calculate the losses in each point of the operational area, is possible to determine the motor's yield in each point. The result of the process as the efficiency maps for each motor is shown in Fig. III-9. The losses calculation are exemplified in chapter III.2.

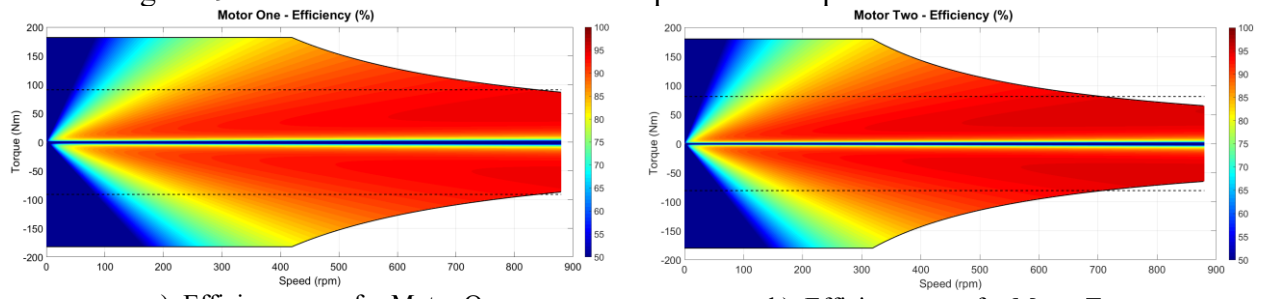

a). Efficiency map for Motor One

b). Efficiency map for Motor Two

Fig. III-9. Efficiency maps of the motors

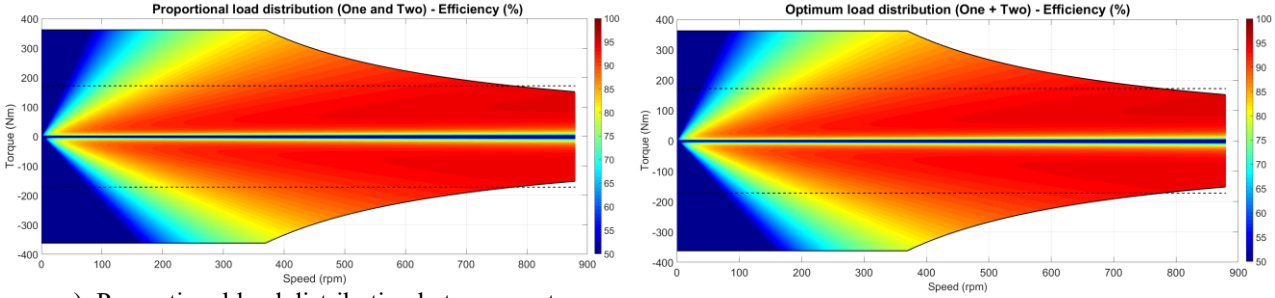

a). Proportional load distribution between motors

b). Optimal load distribution between motors

Fig. III-10. Efficiency map of the powertrain for proportional and optimal load distributions

To illustrate the efficiency improvements with two precedent motors the vehicle from Table II-1

is considered under conditions from Table II-2. Fig. III-11 shows the result.

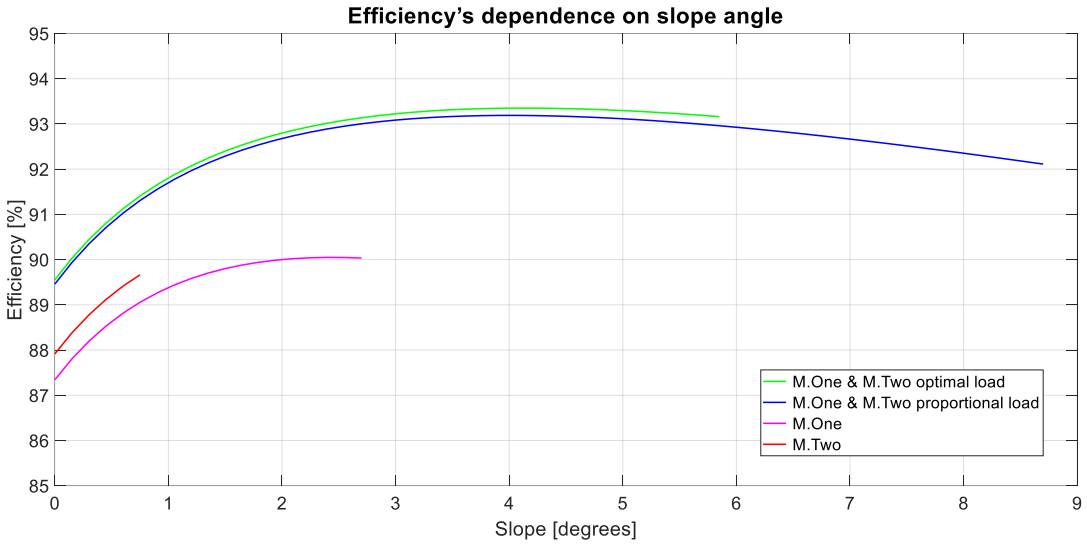

Fig. III-11. Powertrain energetic efficiency after an entire WLTC for 0° to 9° slope angles

III.2. Dynamic load allocation method

III.2.1. Definition

Preserving the vehicle stability, a dynamic load allocation scenario can be defined as a charge repartition algorithm between the motors, calculated in each operating point of the powertrain, considering a specific decision for the operating point and/or considering the previous situations (speed, torque) and the requests for next situations.

III.2.2. Example of load distribution based on motors internal losses minimization

Total losses

The efficiency of a motor *m* is

$$\eta_m = \frac{P_{t_m}}{P_{t_m} + P_{l_m}}, \tag{III-6}$$

where P_{t_m} is the mechanical power at motor shaft, and P_{l_m} the lost power in the motor.

Hysteresis and eddy currents losses

Using the iron losses dependance on speed and square of speed,

$$P_{li_m} = K_{H_m}\Omega_m + K_{F_m}\Omega_m^{\,2}, \tag{III-7}$$

where the hysteresis losses coefficient, K_{H_m} and the eddy currents losses coefficient, K_{F_m} .are calculated for motors in Table II-3, using the process in III-8 resulting the values in the next table.

Table III-3. Iron losses coefficients for studied motors

Characteristics	Motor One	Motor Two
Hysteresis losses coefficient	0.09 W/rpm	0.06 W/rpm
Eddy currents losses coefficient	0.0001 W/rpm^2	0.00009 W/ rpm^2

As a characteristic regarding the optimization process, **these losses do not depend on the load and are present during the whole testing cycle as a function of speed**.

Joule losses

Knowing the internal resistance of each motor, for a given current, the Joule losses can be calculated. During the WLTC the motors must cover the total torque request. Under this constraint is possible to find for each operating point a couple I_1, I_2 minimizing the Joule losses:

$$\min(P_{lJ}) = \min\left(R_1 I_1^{\,2} + R_2 I_2^{\,2}\right). \quad \text{(III-8)}$$

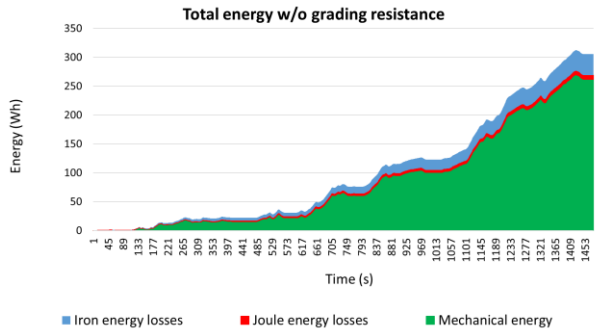

a). on a flat surface with losses minimization

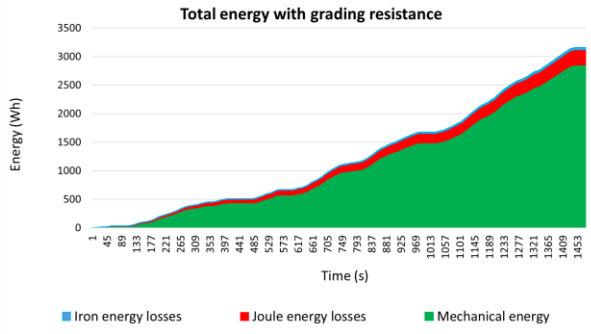

a). on a slope of 15° with losses minimization

Fig. III-12. Total energy during WLTC

Conclusion

In terms of total energy used during the testing cycle, the results obtained for losses minimization have been compared with the results when Motor One covered any time 60% of the load and Motor Two, 40%. Energy efficiency is improved by 0.2 % on a flat surface and 3.4% on a slope of 15 degrees. The coverage of the entire WLTC on a 15 degrees slope is, in this case, a theoretical assumption to illustrate the influence of higher motor currents for this method, as the iron losses are not influenced by the slope angle.

III.3. Mixed load allocation method

III.3.1. Definition

A mixed load allocation is a method which combines the application of static and dynamic load allocation methods.

III.3.2. Extension of the vehicle capabilities using mixed load distribution

Coming back to the case illustrated in Fig. III-11, the optimal load distribution curve stops earlier than the proportional load one, at a smaller slope angle. In fact, for the proportional load distribution, the motors, at least theoretically, arrive at their limits at the same time. It means that the powertrain attempts its limits, and the testing cycle will not be respected entirely. The maximum slope angle attempted using a proportional load distribution is used to understand the situation. At this angle, if the optimal load distribution is applied: the powertrain attempts its limits (Fig. III-13), Motor One still have reserves and can continue to be charged, Motor Two is overloaded (Fig. III-14). It means that Motor Two attempts its limits earlier than Motor One. Starting from a such moment it is not possible to charge more Motor Two. The optimal load repartition cannot be applied further. As the powertrain continues to have capabilities from Motor One, it is still possible to go further increasing the slope angle. The complementary charge which cannot be supported by Motor Two can be affected to Motor One until also Motor One attempts its limits. The solution combines a static load allocation until Motor Two attempts its limits and, after, a dynamic load allocation, Fig. III-15.

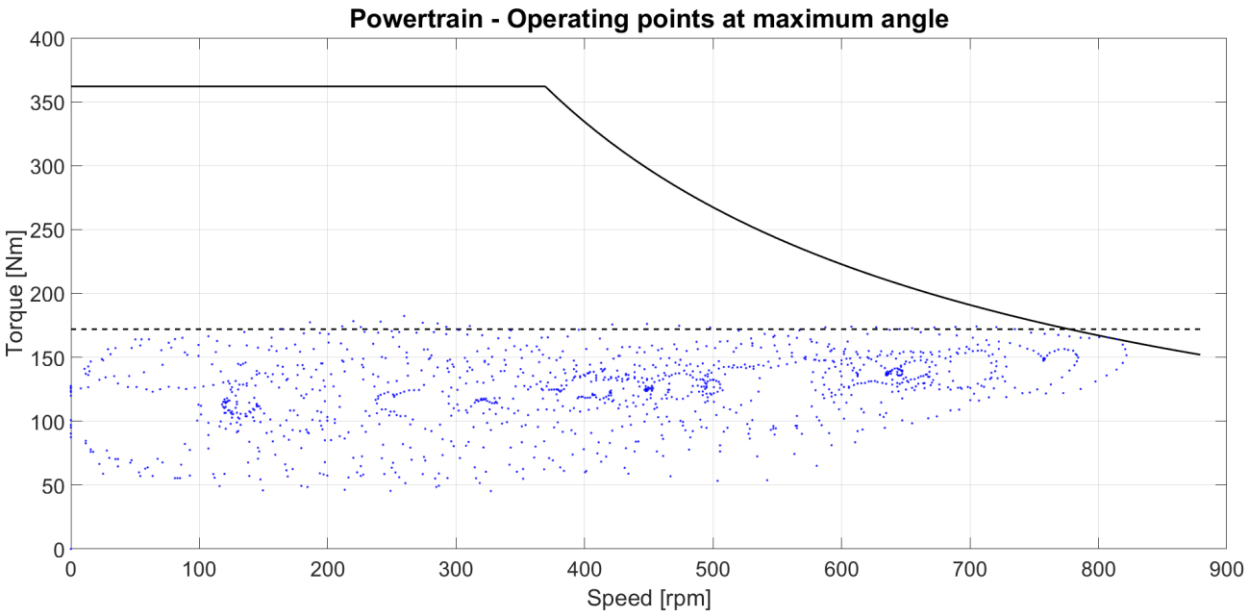

Fig. III-13. Optimal load distribution – powertrain operating points at maximum slope angle

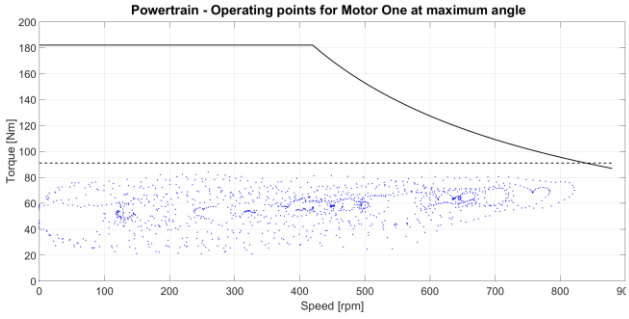

a). Motor One operating points at maximum slope angle

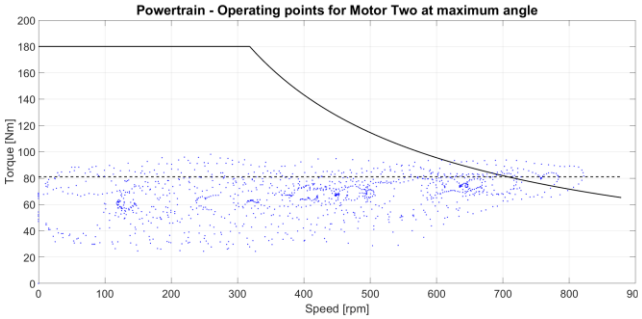

b). Motor Two operating points at maximum slope angle

Fig. III-14. Optimal load distribution

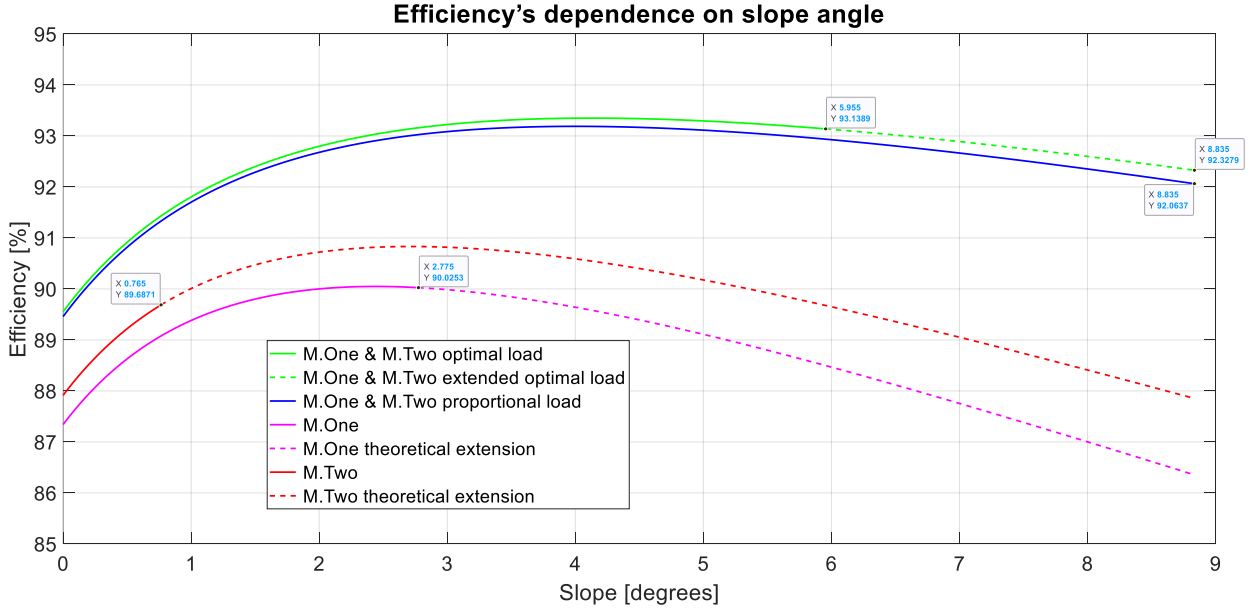

Fig. III-15. Energetic efficiency after an entire WLTC for 0° to 9° slope angles with extension of the optimal load distribution

Conclusion

The advantages of a multi-motor solution are again presented, this time in a mixed load allocation between motors. An extension of the vehicle usage has been realised up to the superior limits of the electric motors. To make more severe the test, a grading resistant force had been considered by an increasing slope angle, and the vehicle powertrain had been optimized using static, dynamic, and mixed load distributions.

III.4. Physical limits for the powertrain

Vehicle from Table II-1 under conditions in Table II-2 are considered for the next study. The motors in Table II-3 are participating to the powertrain. In the case when the vehicle has a towable mass attached, and the towable mass doesn't have a dedicated powertrain, the tractive effort must also cover the resistant forces coming from the towable mass. Considering the maximum torque, the maximum power of the powertrain, and the tractive effort $P_{t_{max}}$, $T_{t_{max}}$, $F_{t_{max}}$, the tractive effort must satisfy the next conditions: $F_t \le F_{t_{max}}$, $F_t \le T_{t_{max}} / r_w$, $F_t \le P_{t_{max}} / \Omega_w r_w$, where r_w and Ω_w are the wheel radius and wheel angular speed. The limits regarding the towable mass are presented in the next figure.

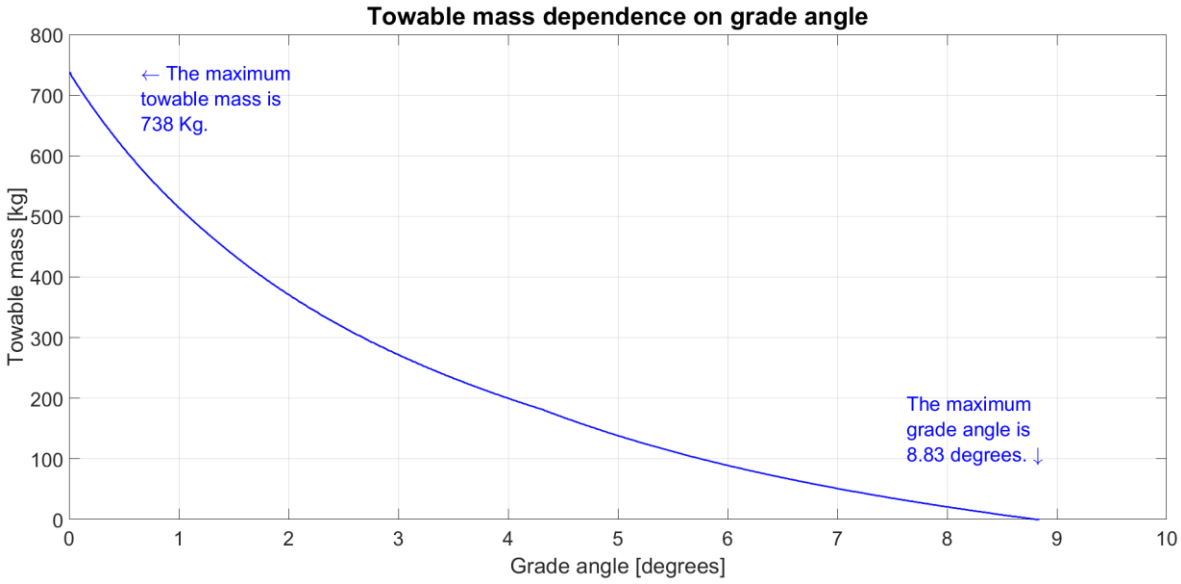

Fig. III-16. Slope angle influence on the towable mass

On a flat surface it results that the vehicle can tow a mass of 738 Kg respecting WLTC. It represents almost three times the vehicle mass. Considering that the minimum mass of the base vehicle is 50 kg the next figure presents the dependence between the basic vehicle mass and the total mass of the ensemble (vehicle + trailer) for different slope angles, also respecting entirely the WLTC.

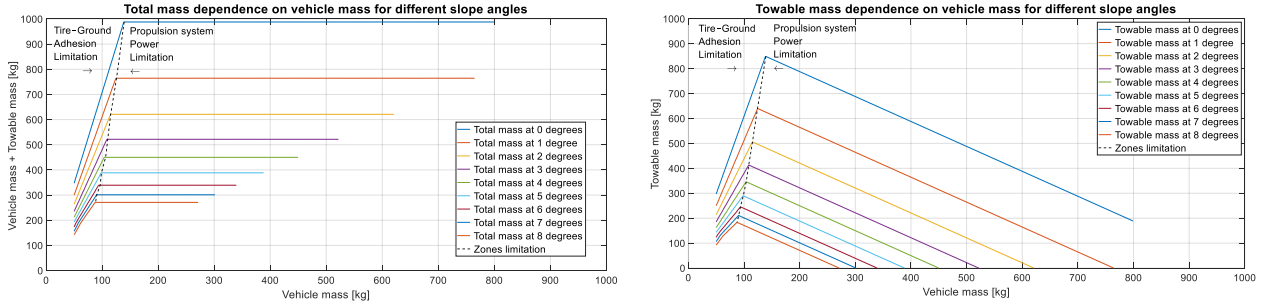

a). Dependence of the vehicle mass on total mass b). dependence of the vehicle mass on towable mass

Fig. III-17. Powertrain limits for the ensemble (vehicle + trailer), for 0° to 8° slope angles

III.5. Conclusions

The simulations realized during the research presented in actual chapter allowed to achieve a double goal: to confirm the positive impact of EV multi-motor powertrains usage in terms of onboard energy efficiency, and to compare the results obtained by different methods. The internal losses of the electric motors have been calculated using the motors' main characteristics and physical dimensions. Also, the method and the calculation for the iron losses coefficients depending on motor speed and square motor speed, have been presented. Several load allocation methods between motors have been identified and analyzed: static load allocation (complementary, percentual, proportional and optimal load distributions), dynamic load allocation (based on past and future situations, using internal motors losses minimization) and mixed load allocation. The optimal load distribution performs better, but the approach of the superior limit of the motors must be supervised as the method can have a shorter area of application as the proportional one. To overcome this limit a mixed load allocation can be successfully applied. Efficiency maps for both cases have been generated, and also for each individual motor. The improvement is more visible on an efficiency representation for increasing slope angles. In complement at the end, it was presented a new method to explore the vehicle capabilities starting from the powertrain characteristics. It represents the construction of vehicle physical limits in terms of vehicle mass and towable mass for different slope angles, under the constraint to respect entirely a given testing cycle.

IV. Optimization Techniques for BLDC Propulsion Systems

IV.1. Constitution of the motor model

Back EMF in three-phase BLDC motor

A usual construction of the motor presents three phases. BLDC motors are designed to develop trapezoidal back EMF, as represented in Fig. IV-1. Between the three phases, the back EMF is shifted by 120 electrical degrees.

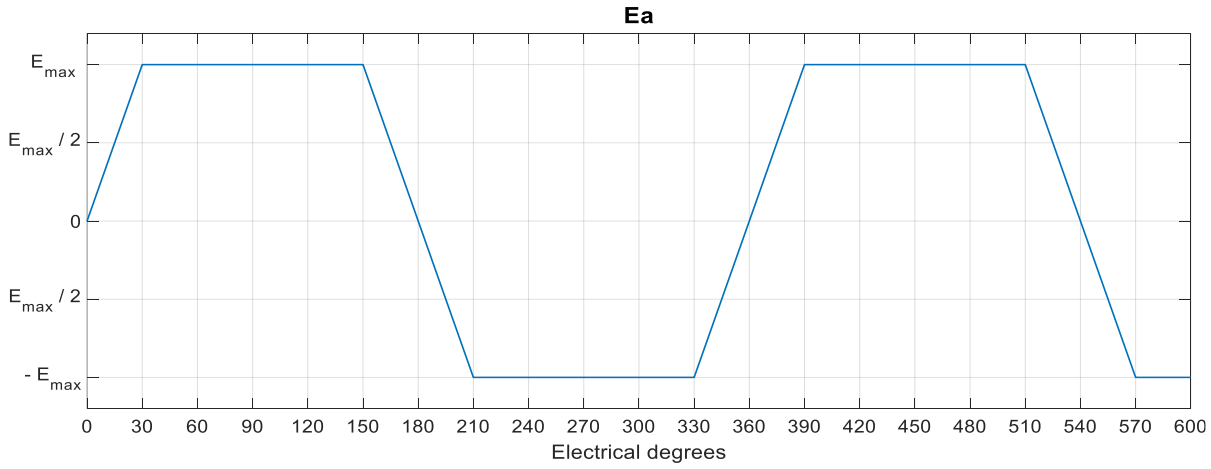

Fig. IV-1. Back electromotive forces: for phase a

BLDC motor model

Modelling the mechanical system

The electromagnetic torque T_E is the rapport between the electromagnetic power and angular speed of the rotor. Using the motor in a vehicle propulsion system, it must cover the torque request,

$$T_E = F_c\Omega + T_{f0} + T_{load} + J\frac{\mathrm{d}\Omega}{\mathrm{d}t}, \qquad \text{(IV-1)}$$

where, F_c is the viscous friction coefficient for motor and load and T_{f0} is the static friction torque (both covers the power losses depending on speed and square of the speed), T_{load} is the necessary load requested by the vehicle to cover the aerodynamic drag, the rolling resistance and grading resistance, J is the inertia of rotor and load, Ω is the angular speed of the rotor. Considering θ the angular position of the rotor:

$$\Omega = \frac{\mathrm{d}\theta}{\mathrm{d}t}. \qquad \text{(IV-2)}$$

IV.2. Ideal and real currents in the motor

By simulation at 500 rpm, it is obtained that the imposed (ideal) current for the phase a, $i_{a\text{-ref}}$ has a rectangular shape, but not the real current i_a. As a result, the electromagnetic torque in the machine is fluctuating around a mean value and the phase commutation generates torque ripples as shown in Fig. IV-4.

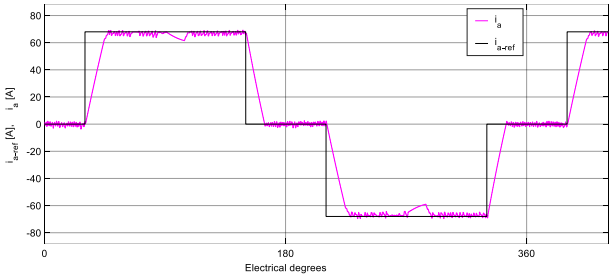

Fig. IV-2. Phases commutation influence on the phase current

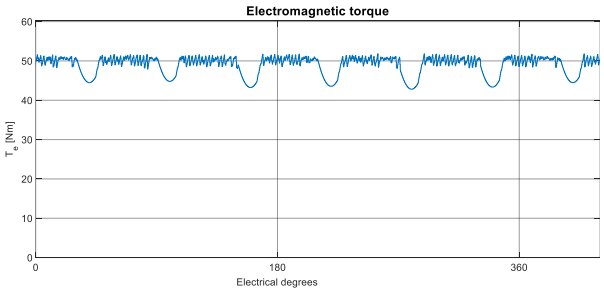

Fig. IV-3. Electromagnetic torque in the motor

<u>Effect of an increased speed</u>

For the same motor, the speed has been increased from 500 rpm to 750 rpm. Consequently, there is an important limitation in the electromagnetic torque and the torque ripples increase significantly.

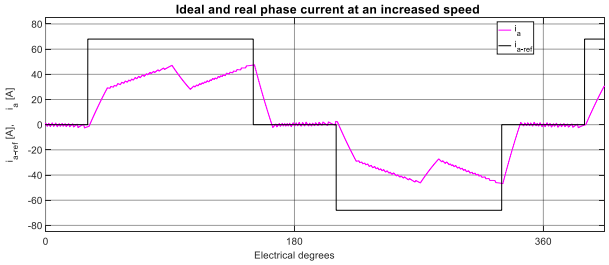

a). Current

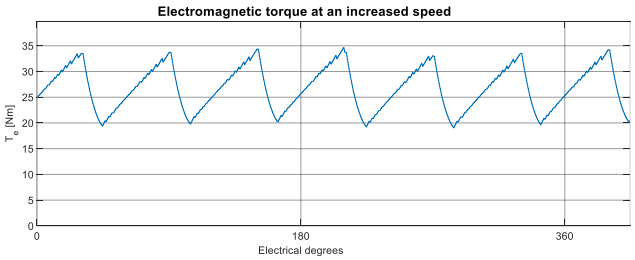

b). Torque

Fig. IV-4. Effect of a speed of 750 rpm

IV.3. Application of Phase Advance and Dwell Control methods

Looking to the precedent figure if the phase a is supplied before the moment when the phase back EMF has already attempted the maximum value, this is conductive to favorize the increasing of the current through phase a. In this case the ideal phase current pulse can be advanced by 60 degrees and can last a maximum of 180 degrees. The technique of advancing the commutation signal to open the phase current is called **Phase Advance** (PA). The technique of delaying the commutation signal to

stop the phase current is called **Dwell Control** (DC). **The difference from precedent research consists in proposing a propulsion system with two identical BLDC motors, trying to use an appropriate configuration to the smallest one. Each motor has the characteristics specified in Table IV-1.**

Table IV-1. Characteristics of the motors for PA and DC investigations

Characteristics	Values
Nominal power	3 kW
Maximum power	5,4 kW
Nominal voltage	72 V
Pair poles	16
Nominal current	68 A
Nominal speed	650 rpm
No load speed	860 rpm
Stator Phase resistance	0.027 Ω
Stator Phase inductance	0,15 mH

MATLAB-Simulink model for operational area investigation

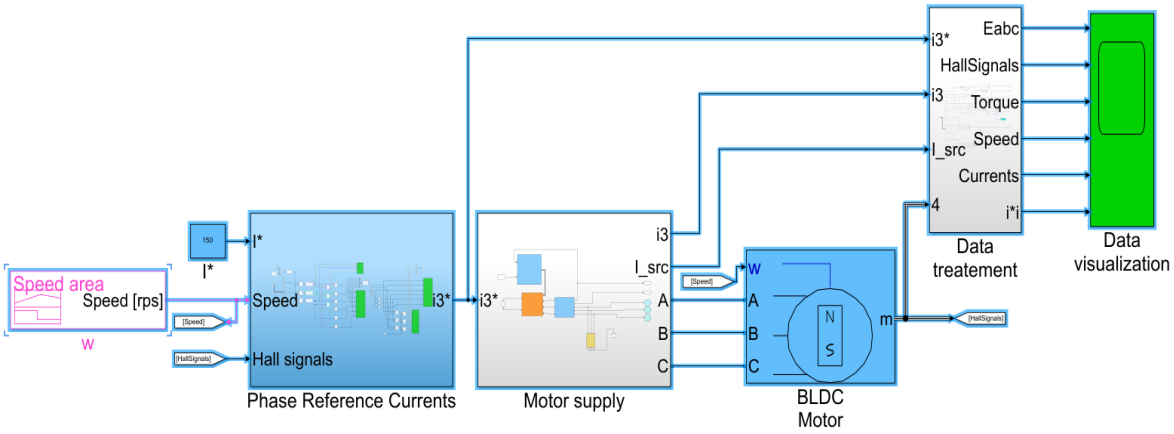

Fig. IV-5. Simulink implementation for operational area coverage

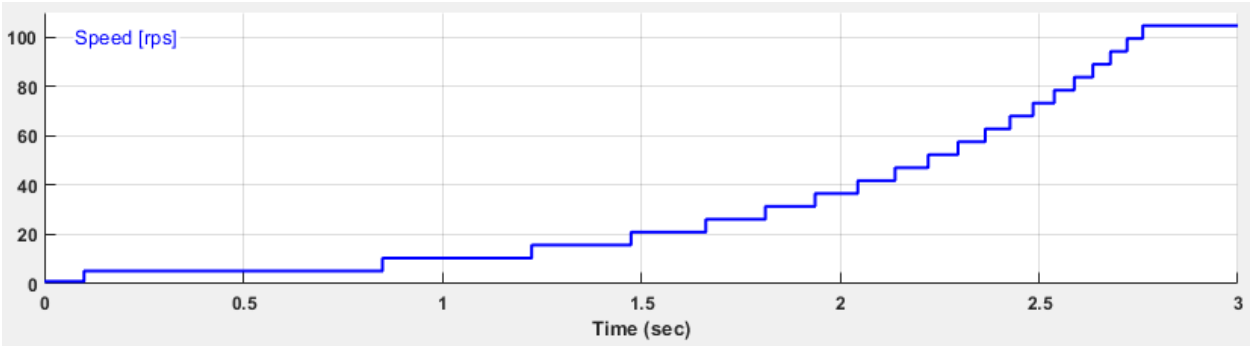

Fig. IV-6. Motor speed profile for operational area investigation

The "Phase Reference Currents" block, based on motor speed and Hall signals, generates the ideal rectangular shape of phase currents with a phase shift of 120 degrees. The amplitude is the imposed value for the current provided by the source. The next figure presents the shape of Hall signals and reference currents for an imposed current at nominal value (68 A). In "Motor Supply", the inverter connected to the voltage source receives the commutation pulses from the regulator. The regulator compares for each phase the real current to the reference current and generates the commutation pulses. The "BLDC Motor" simulates a trapezoidal back-EMF permanent magnet synchronous motor,

supplied in direct current. The "Data Treatment" block generates the data for the investigation. From the electromagnetic torque, subtracting the equivalent torque produced by friction and iron losses torque, it results the shaft torque. Applying the method presented in chapter III the equivalent static torque obtained is T_{f0} = 0.89 Nm and the equivalent coefficient of viscous friction F_c = 0.021 Nms. A three-phase MOSFET/Diodes inverter ("Power electronics block" in Fig. IV-7) supplies the motor.

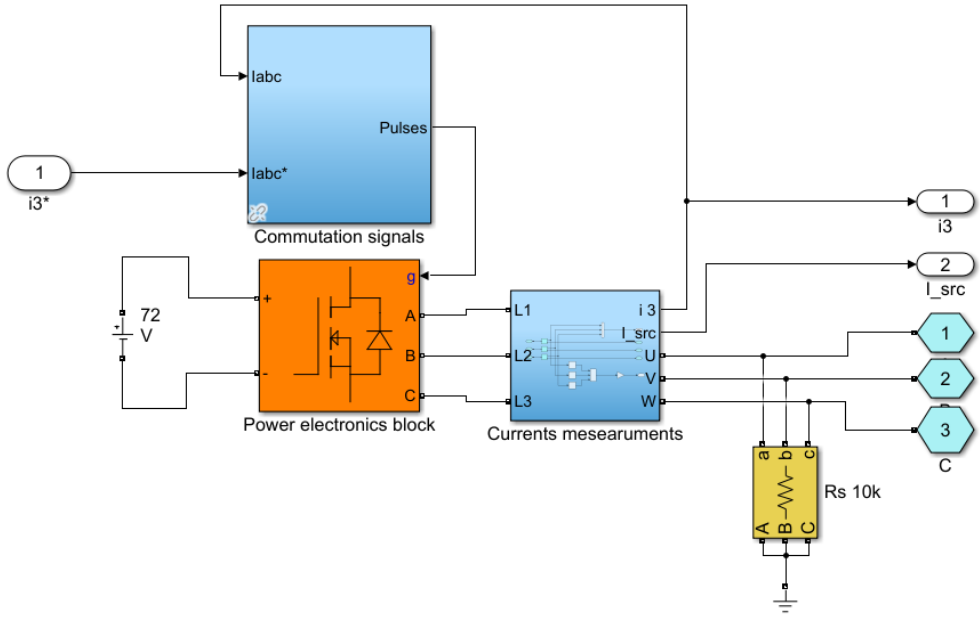

Fig. IV-7. "Motor Supply" block

Vehicle request for operational area coverage

The maximum power of the motor (5.4 kW) is obtained at speed of n = 550 rpm and for a maximum current of I = 136 A. The operating points requested for the propulsion system are superposed on the operational area generated by the two identical motors. The results are shown in Fig. IV-9 without grading resistance and respectively in Fig. IV-10, at eleven-degree slope. Without grading resistance, the operating point at 800.6 rpm requests a torque of 53.6 Nm. Running the simulation at this speed for the maximum current as reference (136 A), the propulsion system with two identical motors can provide only 25.75 Nm. Imposing a higher reference current will not change the current in the motor.

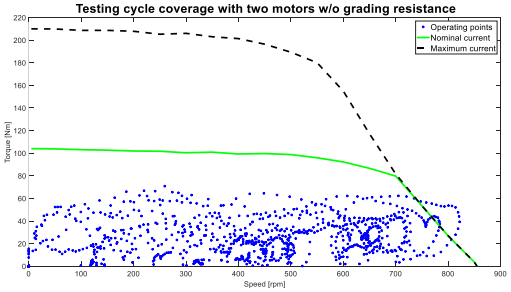

Fig. IV-8. Propulsion system operational area and operating points request without grading resistance

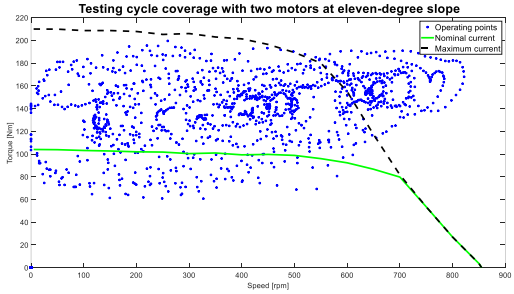

Fig. IV-9. Propulsion system operational area and operating points request for 11° slope angle

The situation is worst with grading resistance for a slope angle of 11 degrees. **In this context the research for improvement will not be done by replacing one of the motors by a more convenient one to cover the high-speed region. Both identical motors are kept, and PA and DC are applied for optimization.**

Implementation of PA and DC methods for the investigations

In the next figure the main components of the implementation schema are represented.

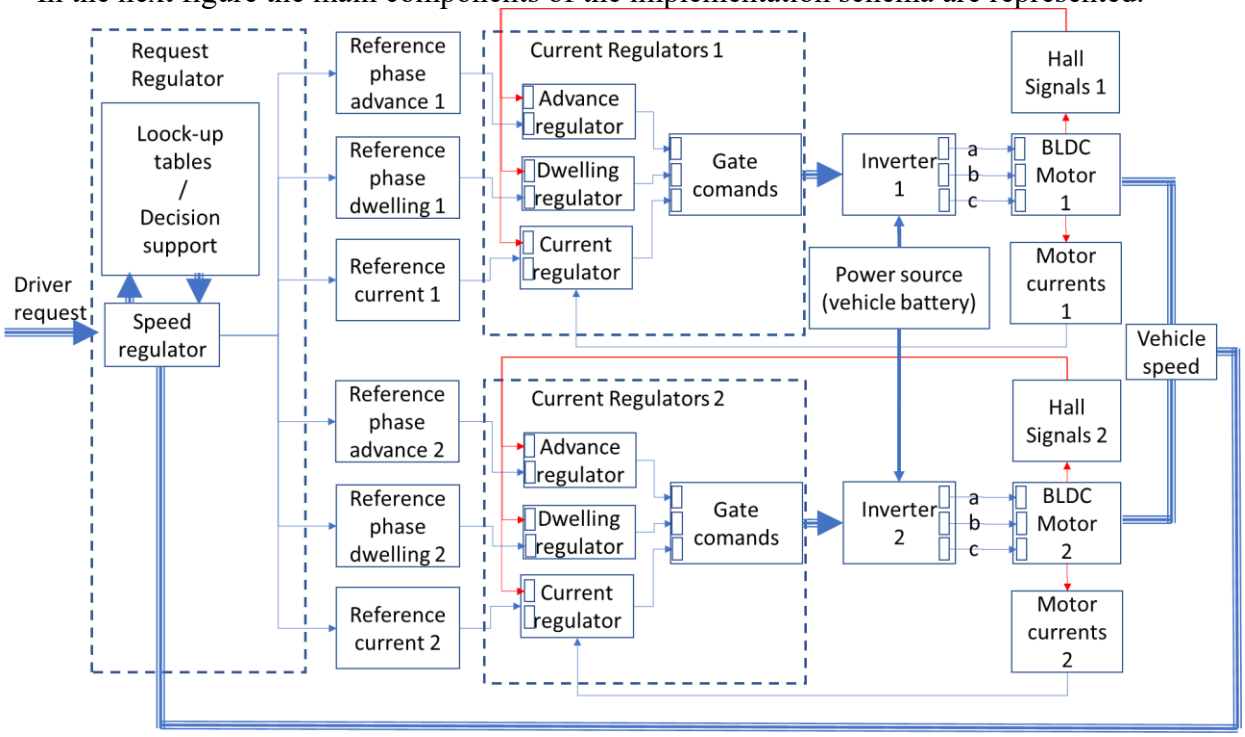

Fig. IV-10. General view on the implementation schema PA and DC methods analysis

Mathematical models for PA and DC for MATLAB-Simulink implementation

To an angle, α_{adv} in electrical degrees (max 60°), corresponds a phase advance, τ_{adv}, in seconds. From the moment when the Hall signal passes to "1", the next passage of the reference current from 0 to $I_{a\text{-}ref}$, is delayed, in seconds, by

$$\tau - \tau_{adv} = \frac{2\pi}{p \cdot \Omega} \cdot \frac{360 - \alpha_{adv}}{360}, \qquad \text{(IV-3)}$$

where p is the number of pole pairs and Ω the angular speed. The dwell control consists in extending the period of time with max 60°, when the phase reference current is at its maximum ($I_{a\text{-}ref}$, for positive pulses and $-I_{a\text{-}ref}$, for negative ones); this period is usually 120 electrical degrees, or $\tau/3$ seconds. By applying a DC angle, α_{dwl}, it is extended by τ_{dwl} seconds. The dependence between the additional time, τ_{adv}, and the DC angle, α_{dwl}, and is

$$\tau_{dwl} = \frac{2\pi}{p \cdot \Omega} \cdot \frac{\alpha_{dwl}}{360}. \qquad \text{(IV-4)}$$

IV.4. Conclusion

This chapter has introduced the PA and DC methods applied in the supplied voltage commutation between the phases of the motor, explaining the commutation periods and the consequent impacts. Based on simulation the results are confirmed. The methodology for implementation was explained and the mathematical model for PA and DC angle calculation introduced for building the Simulink model. The improvements obtained using these methods are presented in the next chapter.

V. INFLUENCE OF PA AND DC METHODS ON BLDC PROPULSION SYSTEMS

V.1. PA results on operational area coverage

For simplification, it is considered that the same PA angle is applied to each motor of the powertrain and the method is used starting from a motor speed of 50 rpm.

Results obtained for the maximum reference current

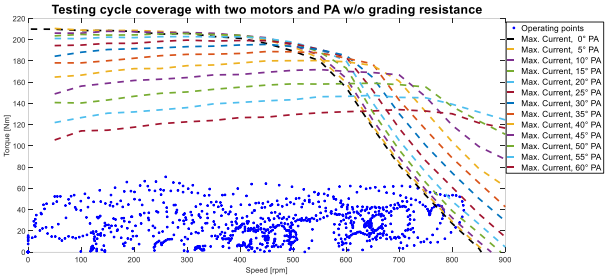

Fig. V-1. Influence of the PA angle on operational area coverage, case without grading resistance

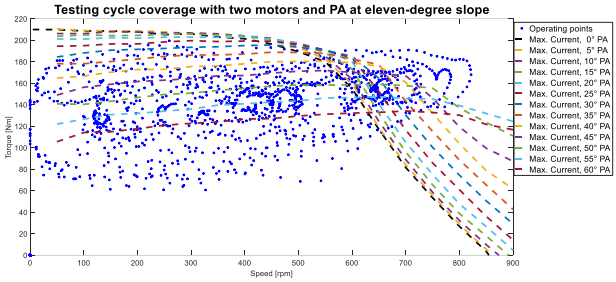

Fig. V-2. Influence of the PA angle on operational area coverage, at 11° slope angle

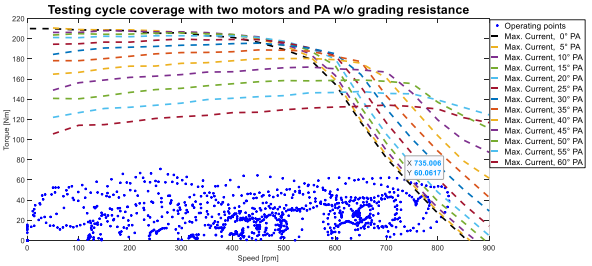

Fig. V-3. Operational area coverage with a PA angle of 25° for more than 735 rpm, w/o grading resistance

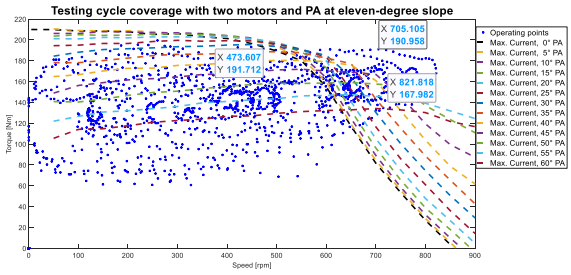

Fig. V-4. Operational area with PA – limits for uncovered operating points

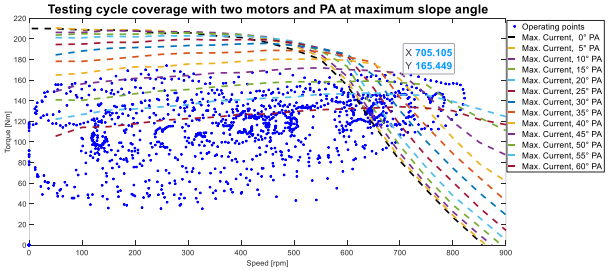

Fig. V-5. Operational area with PA – maximum slope angle (8.8°) for the coverage of maximum local torque at high speeds

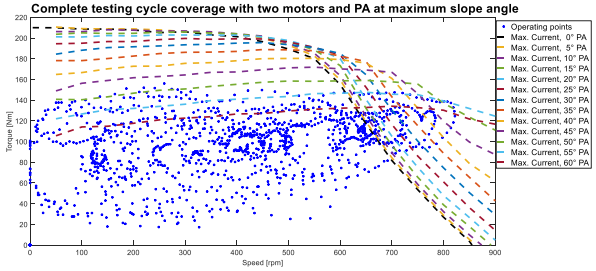

Fig. V-6. Complete operational area coverage with PA for a maximum slope angle of 7.2°

Results obtained for the nominal reference current

The operational area is covered for a PA angle of 25°. **From the resulting data is determined that the application of PA would be necessary for more than 735 rpm.**

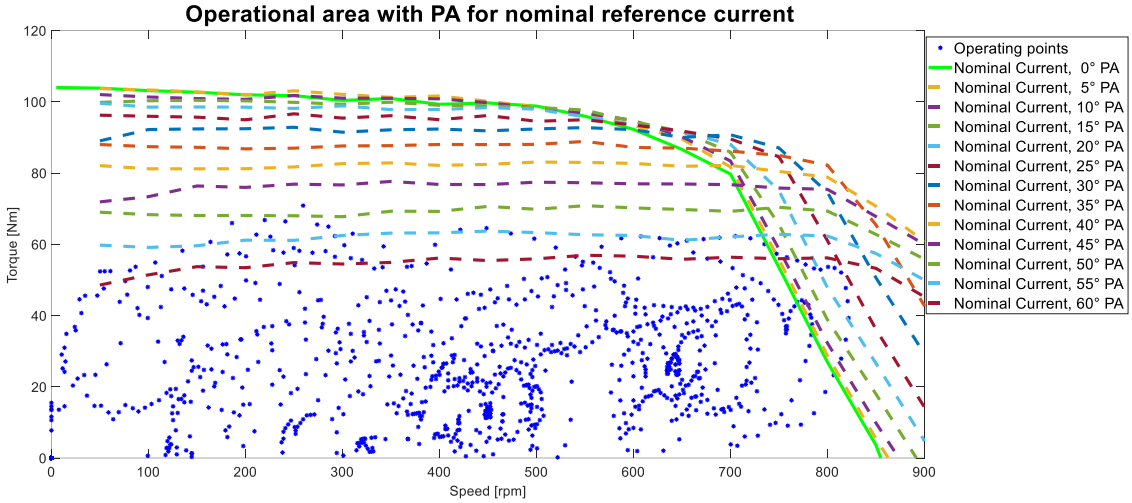

Fig. V-7. Operating points coverage using PA for nominal reference current

Maximum speed investigation

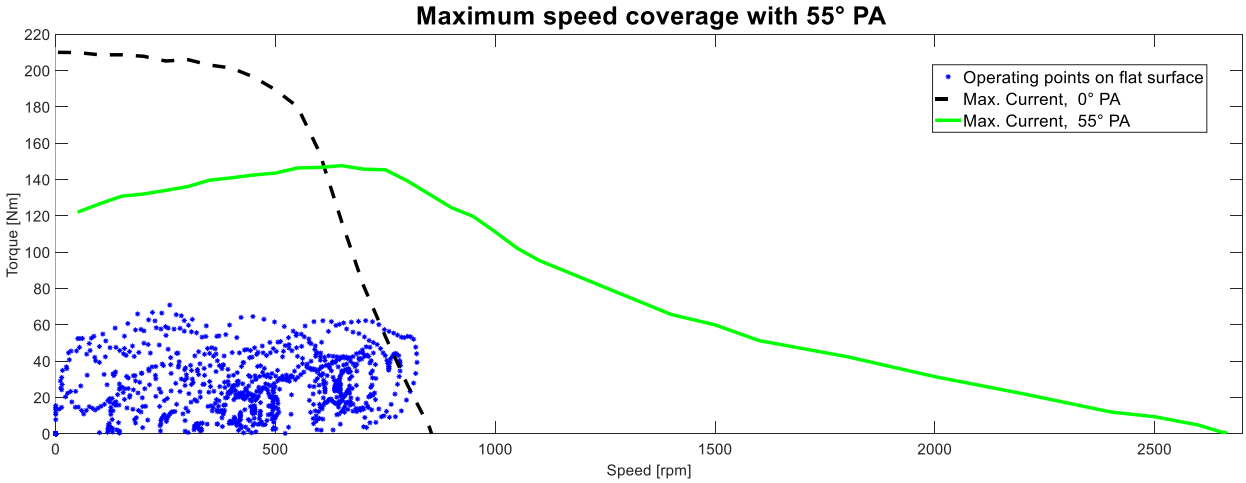

Fig. V-8. Operating points coverage using PA for maximum reference current

Influence on the motor currents

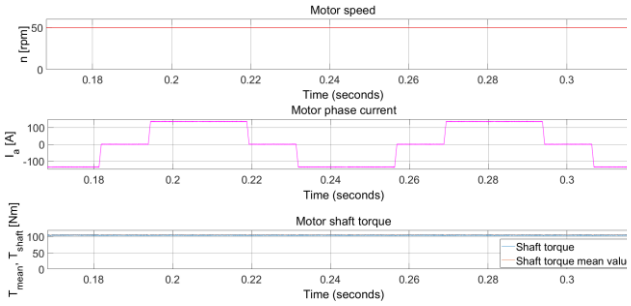

Fig. V-9. Phase current and torque for maximum reference current (136 A) without PA at 50 rpm

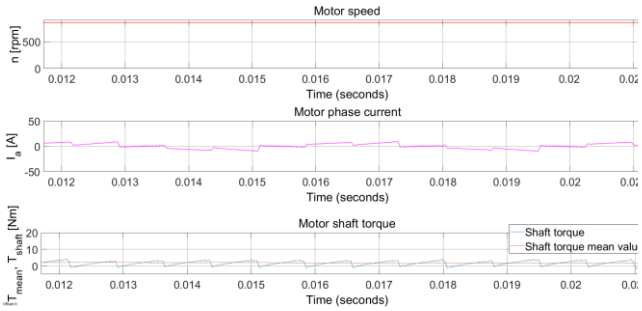

Fig. V-10. Phase current and torque for maximum reference current (136 A) without PA at 850 rpm

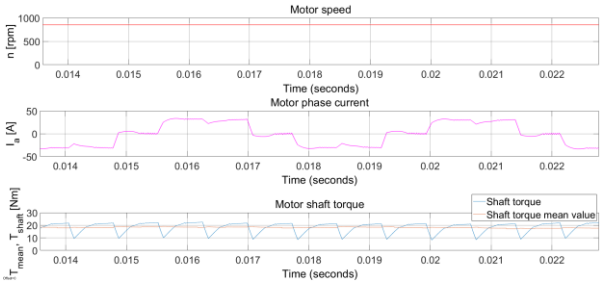

Fig. V-11. Phase current and torque for maximum reference current (136 A) and 25° PA at 850 rpm

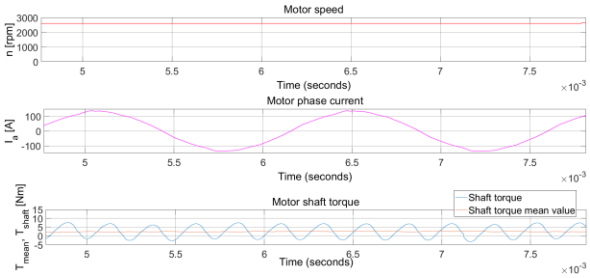

Fig. V-12. Phase current and torque for maximum reference current (136 A) and 55° PA at 2600 rpm

V.2. Operational area coverage by completing PA with DC

Results obtained for the maximum and nominal reference current

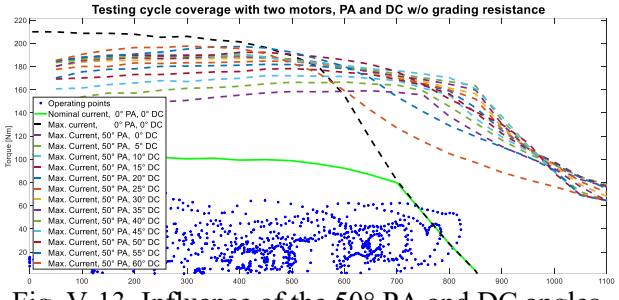

Fig. V-13. Influence of the 50° PA and DC angles on operational area coverage, case without grading resistance

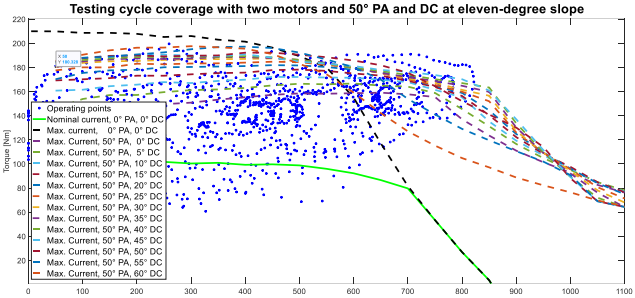

Fig. V-14. Influence of the 50° PA and DC angles on operational area coverage, at 11° slope angle

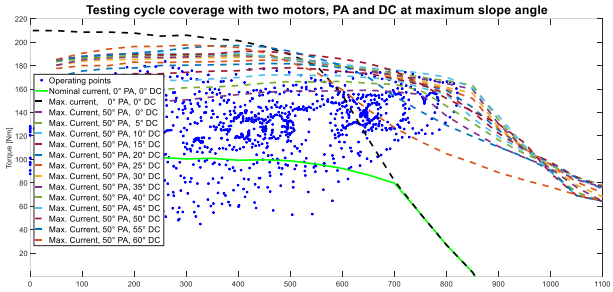

Fig. V-15. Complete operational area coverage with 50° PA and DC for a maximum slope angle of 9.6°

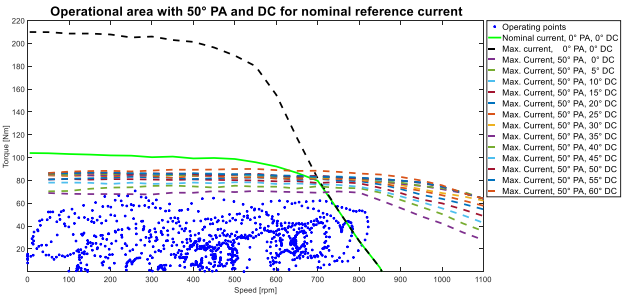

Fig. V-16. Operating points coverage using 50° PA and DC for nominal reference current

Influence on the motor currents

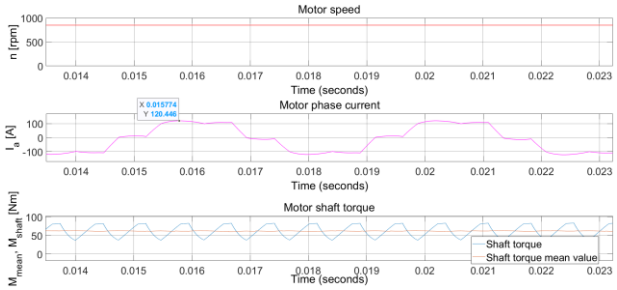

Fig. V-17. Phase current and torque for maximum reference current (136 A) at 850 rpm, 50° PA, 0°DC

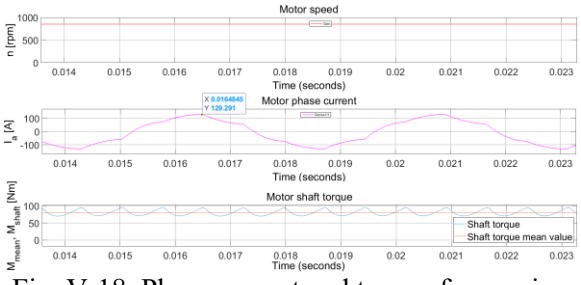

Fig. V-18. Phase current and torque for maximum reference current (136 A) at 850 rpm, 50° PA, 45°DC

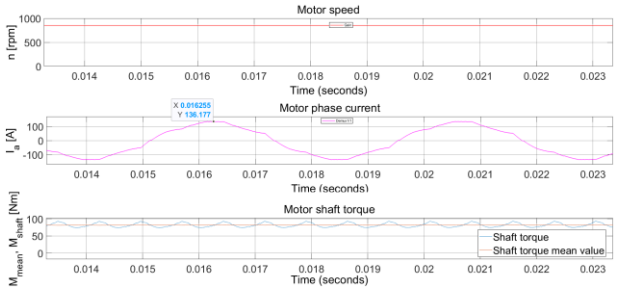

Fig. V-19. Phase current and torque for maximum reference current (136 A) at 850 rpm, 55° PA, 45°DC

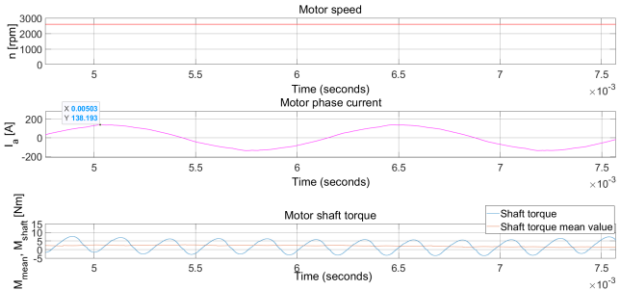

Fig. V-20. Phase current and torque for maximum reference current (136 A) at 2600 rpm, 55° PA, 45°DC

V.3. Impacts on powertrain torque and efficiency

Torque maximization

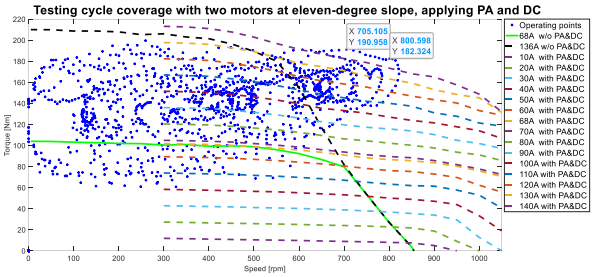

Fig. V-21. Maximum torque curves using PA and DC for 0 to 140A reference current levels with grading resistance

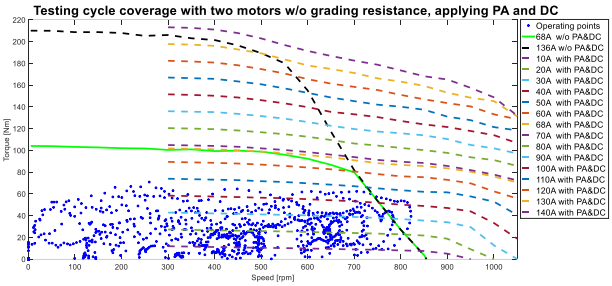

Fig. V-22. Maximum torque curves using PA and DC for 0 to 140A reference current levels w/o grading resistance

Table V-1. Pair of PA and DC angles for WLTC coverage at 50 A

Speed [rpm]	300	350	400	450	500	550	600	650	700	750	800	850	900	950	1000
PA angle [°]	15	15	15	15	20	20	20	25	30	35	35	35	45	45	45
DC angle [°]	15	15	10	15	15	15	20	25	20	20	15	50	60	60	60

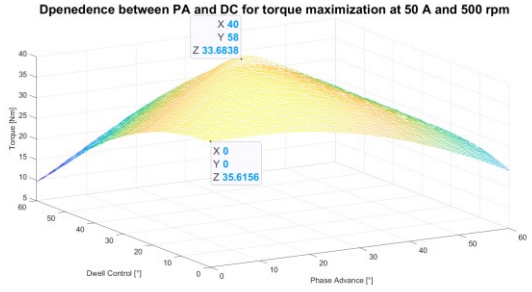

Fig. V-23. Dependence between PA and DC angles for torque maximization at 50 A and 500 rpm

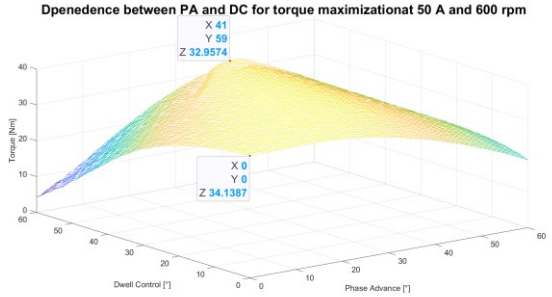

Fig. V-24. Dependence between PA and DC angles for torque maximization at 50 A and 600 rpm

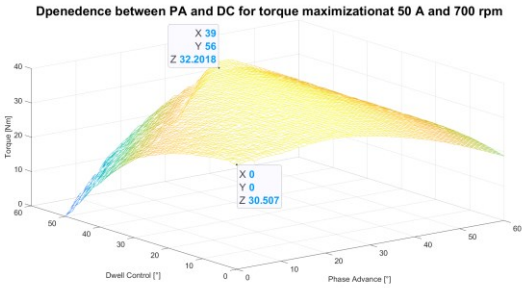

Fig. V-25. Dependence between PA and DC angles for torque maximization at 50 A and 700 rpm

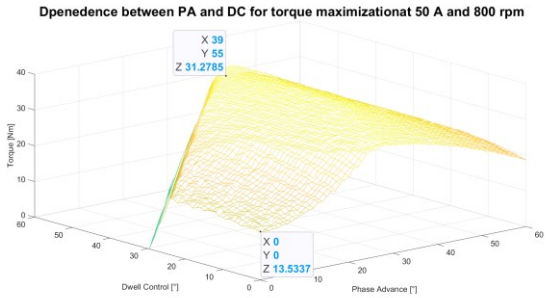

Fig. V-26. Dependence between PA and DC angles for torque maximization at 50 A and 800 rpm

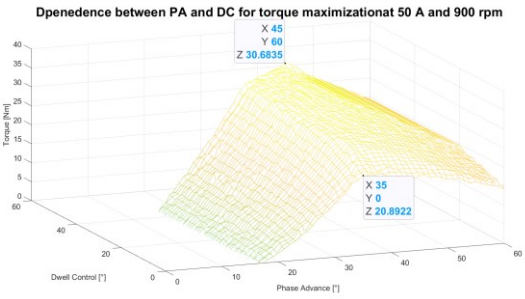

Fig. V-27. Dependence between PA and DC angles for torque maximization at 50 A and 900 rpm

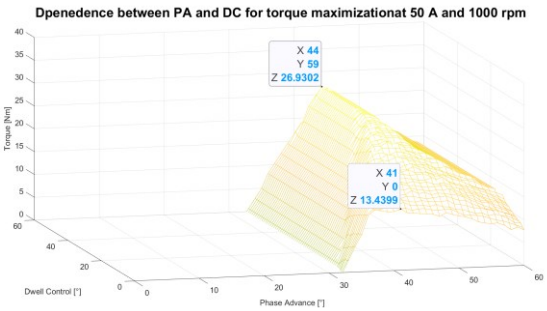

Fig. V-28. Dependence between PA and DC angles for torque maximization at 50 A and 1000 rpm

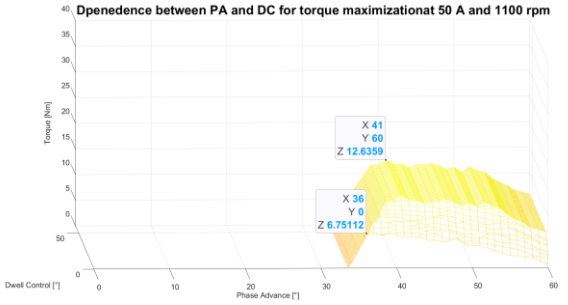

Fig. V-29. Dependence between PA and DC angles for torque maximization at 50 A and 1100 rpm

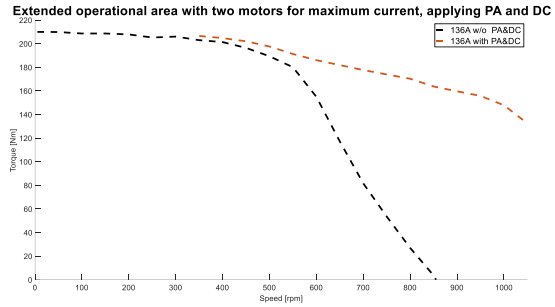

Fig. V-30. Extended operational area at 136 A with PA & DC

Table V-2. Pair of PA and DC angles for powertrain operational area extension

Speed [rpm]	**300**	**350**	**400**	**450**	**500**	**550**	**600**	**650**	**700**	**750**	**800**	**850**	**900**	**950**	**1000**
PA angle [°]	15	15	20	20	30	55	40	45	55	60	55	55	60	60	60
DC angle [°]	5	5	10	0	10	55	40	40	50	55	45	45	50	45	30

Efficiency / Yield maximization

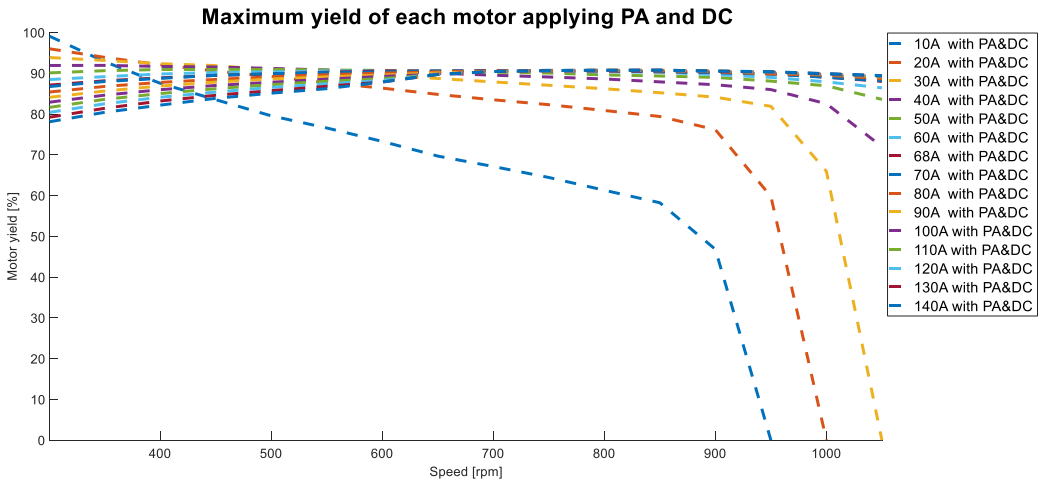

Fig. V-31. Motor maximum yield using PA and DC methods

Table V-3. Pair of PA and DC angles for motors yield optimization at 70 A

Speed [rpm]	**300**	**350**	**400**	**450**	**500**	**550**	**600**	**650**	**700**	**750**	**800**	**850**	**900**	**950**	**1000**
PA angle [°]	10	10	5	10	35	30	25	30	35	30	35	45	45	50	50
DC angle [°]	0	0	0	0	45	30	20	35	40	35	40	55	55	60	40

V.4. PA and DC for energy efficiency improvement in an EV BLDC Powertrain

V.4.1. Entry data for the investigation

Table V-4. Vehicle characteristics for energy efficiency improvement analysis using PA and DC

Characteristic	**Value**	**Measurement Unit**
Maximum mass	250	kg
Wheel radius	0.275	m
Aerodynamic drag coefficient	0.46	-
Frontal area	0.95	m^2
Transmission rapport motor to wheel	1	-

Table V-5. Resistant forces coefficients for energy efficiency improvement using PA and DC

Characteristic	**Value**	**Measurement Unit**
Tractive effort coefficient	0.8	-
Rolling resistance coefficient	0.013	-

Table V-6. Motors characteristics for energy efficiency improvement analysis using PA and DC

Characteristics	**Values**
Nominal power	3 kW
Maximum power	5.4 kW

Nominal voltage	72 V
Pair poles	16
Nominal current	68 A
Nominal speed	650 rpm
No load speed	860 rpm
Stator Phase resistance	0.027 Ω
Stator Phase inductance	0.15 mH

A testing cycle, WLTC (Fig. II-3) is also used in this case to verify the vehicle capabilities.

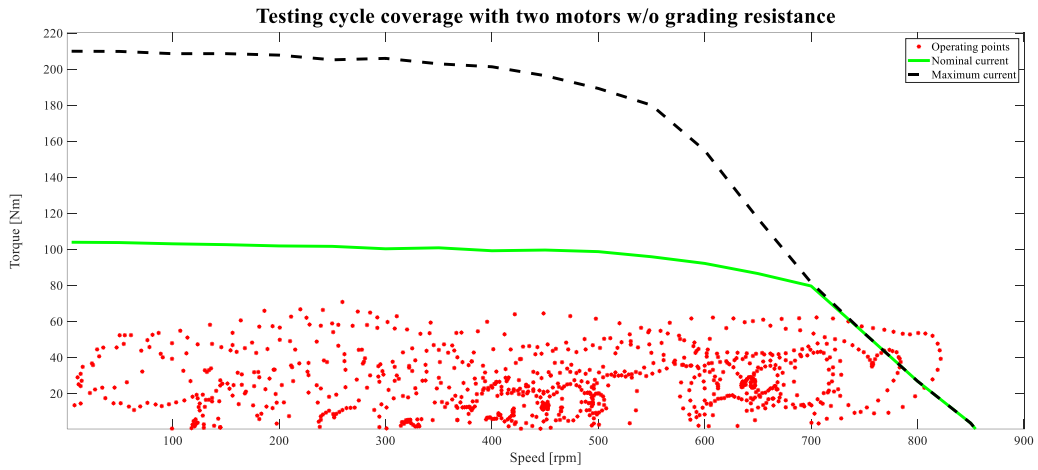

Fig. V-32. Propulsion system operational area and operating points request without grading resistance

V.4.2. Improving the energy efficiency usage in each operating point

Implementation of the testing platform

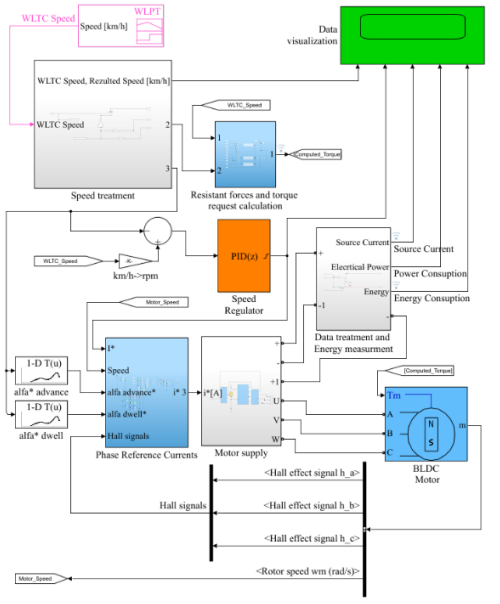

Fig. V 33. Torque-controlled PM BLDC model implemented with PID speed control regulator for improvement confirmation

PA and DC angle calculation for maximum efficiency

The model built in Fig. IV-5 is used for the present investigation with the goal of extending the operational area coverage of the powertrain.

Table V-7. PA and DC angles for maximum efficiency of each motor

Speed [rpm]	**300**	**350**	**400**	**450**	**500**	**550**	**600**	**650**
PA angle [°]	10	10	5	10	35	30	25	30
DC angle [°]	0	0	0	0	45	30	20	35

Speed [rpm]	**700**	**750**	**800**	**850**	**900**	**950**	**1000**
PA angle [°]	35	30	35	45	45	50	50
DC angle [°]	40	35	40	55	55	60	40

V.4.3. Results

Results obtained without the application of PA and DC methods

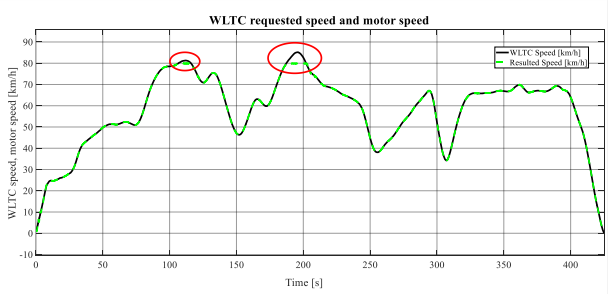

Fig. V-33. Requested speed (in black) and obtained speed (in green) without PA and DC (classic control)

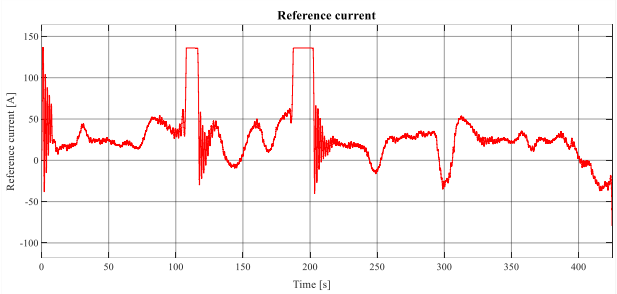

Fig. V-34. Reference current generated by the regulator without PA and DC (classic control)

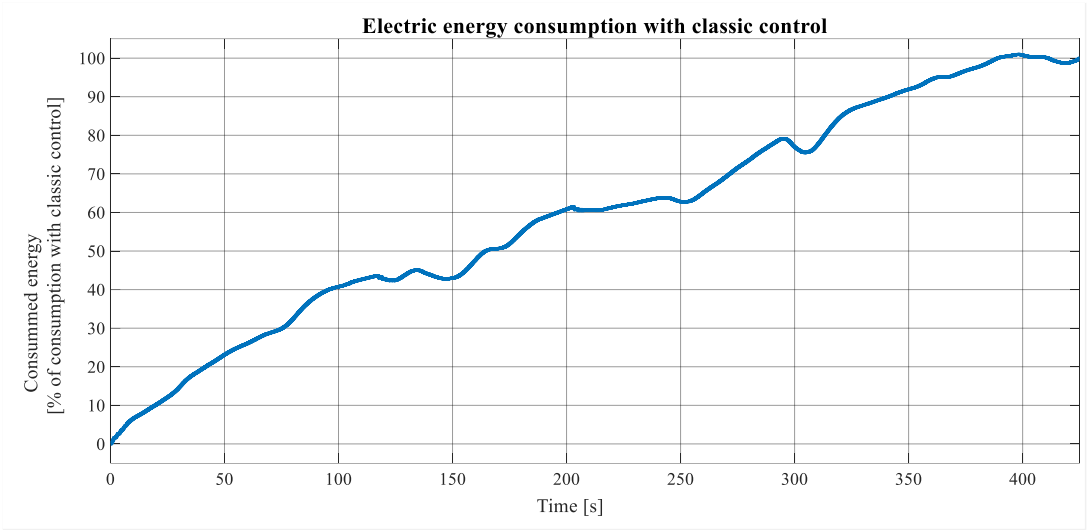

Fig. V-35. Energy consumption without PA and DC (classic control)

Results obtained with the application of PA and DC methods

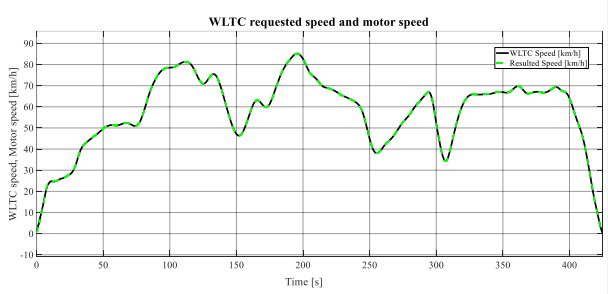

Fig. V-36. Requested speed (in black) and obtained speed (in green) with PA and DC

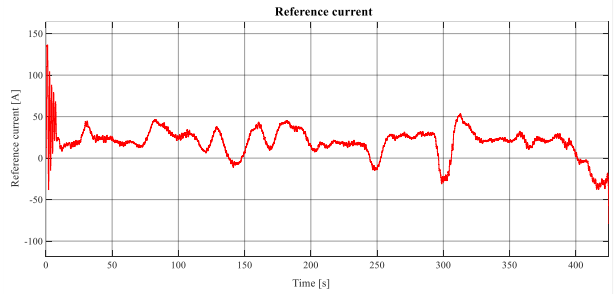

Fig. V-37. Reference current generated by the regulator with PA and DC

The amount of electric energy consumed applying PA and DC methods is smaller, attempting **82.05%** of the total energy consumed using the classic control (without PA and DC). The obtained speed error is about $5 \cdot 10^{-2}$ km/h.

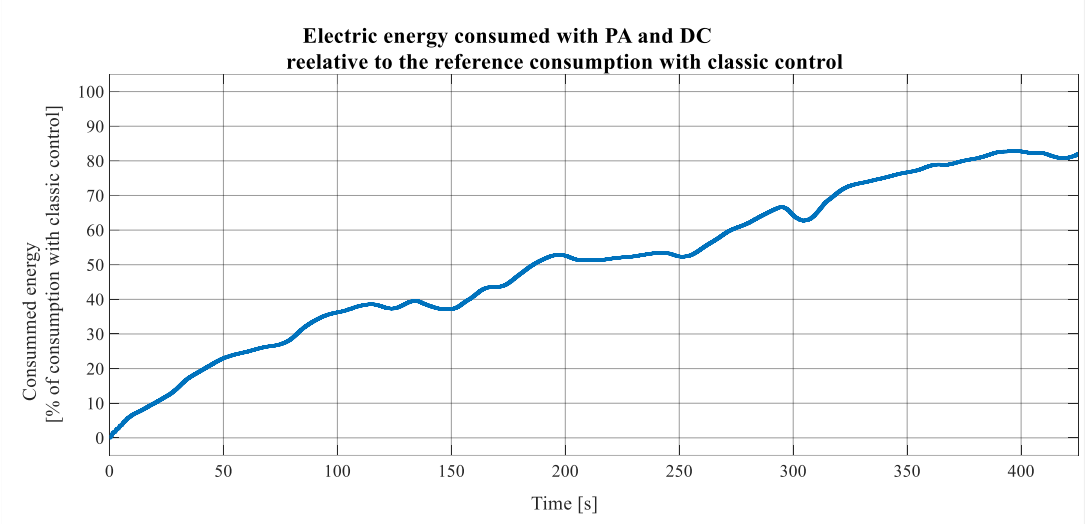

Fig. V-38. Energy consumption with PA and DC

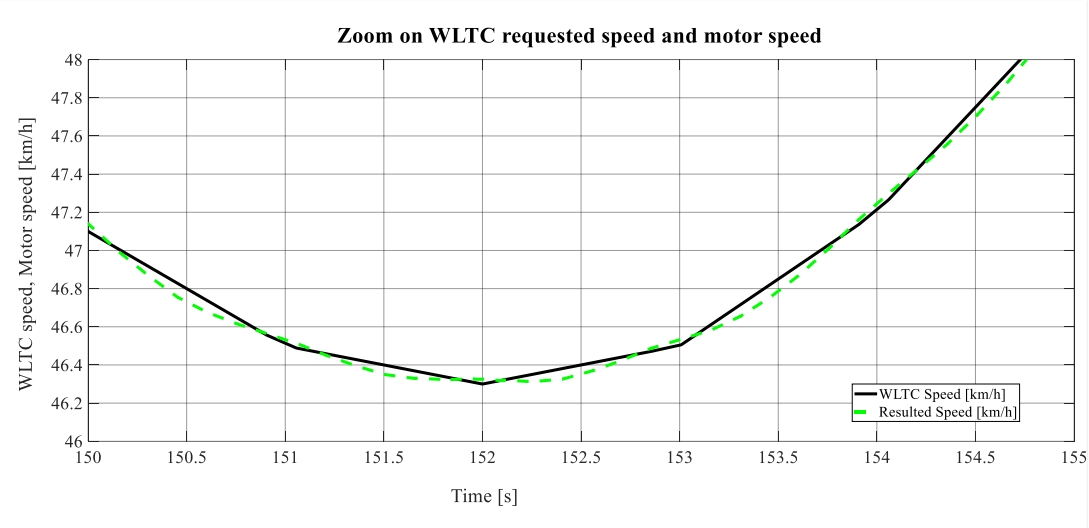

Fig. V-39. Speed regulation with PA and DC

V.5. Conclusions

Applying an advance for the opening of the phase current has generally a negative effect for low-speed regions. For high-speed, the method allows more torque creation, successfully using the period when the back EMF is increasing from zero to its maximum value. The commutation between phases with PA also generates torque fluctuations. Completing PA by delaying the moment when the current is interrupted for a phase, allows the initial current to continue to decrease when the other phase starts to work in parallel. The interruption of the initial current is realized when the current level is lower, and the torque ripples decrease. The right PA-DC couple for a certain reference current at a certain speed generates the requested torque to cover the respective operating point. Regarding speed capabilities, the maximum speed increases quite interestingly using PA (>2600 rpm). At this speed the DC angle had no additional influence. The application of PA and DC methods allows the extension of the operational area of the powertrain, regarding torque maximization, but can be applied also to maximize the efficiency of each motor integrating the powertrain. The pairs of PA-DC angles for a specified reference current have been determined to maximize the motor yield. Finally, it was possible to confirm that the application of an appropriate PA-DC angles in high-speed region can generate positive results for the performance of the powertrain and reduces the energy consumption.

VI. ANALYSIS OF EFFICIENCY MAPS REALIZATION METHODS FOR PM MOTORS. IMPACT OF ADDITIONAL SIMILAR MOTORS ON AN EV POWERTRAIN. COMPLEMENTS TO CHAPTER THREE

The BLDC motor from Table IV-1 is studied from the point of view of efficiency maps realization, comparing analytical calculation and simulation, integrating experimental experience, verifying the optimal load distribution results in a powertrain configuration with three identical motors.

VI.1. Analytic results

Total losses

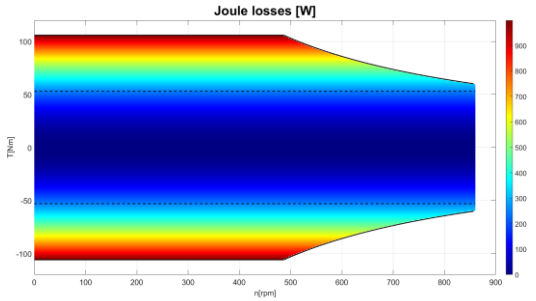

Fig. VI-1. Joule losses – analytical calculation

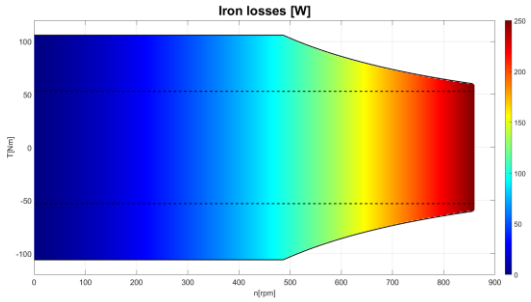

Fig. VI-2. Iron losses – analytical calculation

The iron losses represent the losses by hysteresis and eddy currents. Fig. VI-2 presents the result obtained by calculation and interpolation (process presented in Fig. III-8). Additional losses in the motor (anomalous loss due to different causes) are neglected. The total losses in the motor result as the sum of Joule losses and Iron losses.

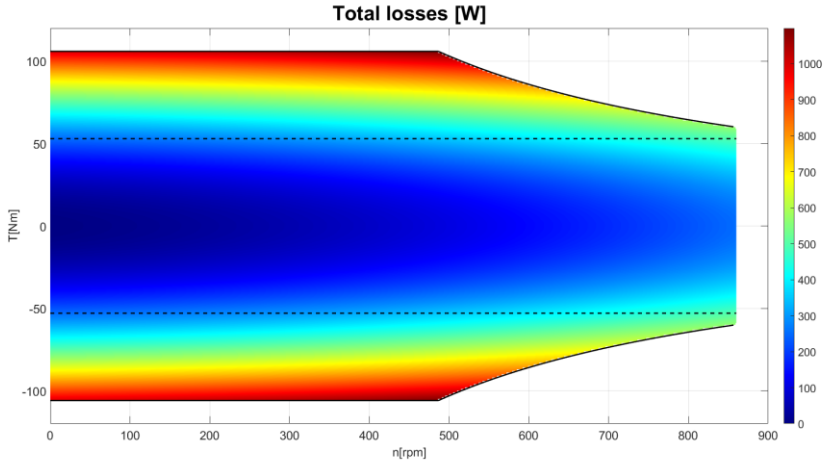

Fig. VI-3.

Fig. VI-3. Total losses – analytical calculation

Output power (mechanical power) and input power (electrical power)

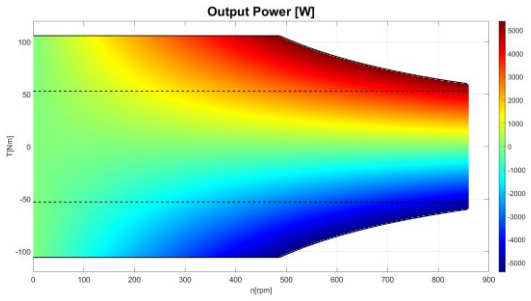

Fig. VI-4. Output power– analytical calculation

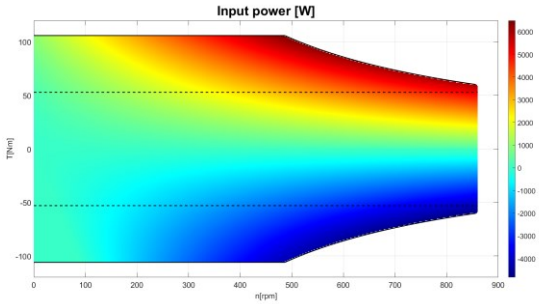

Fig. VI-5. Input power– analytical calculation

Efficiency maps

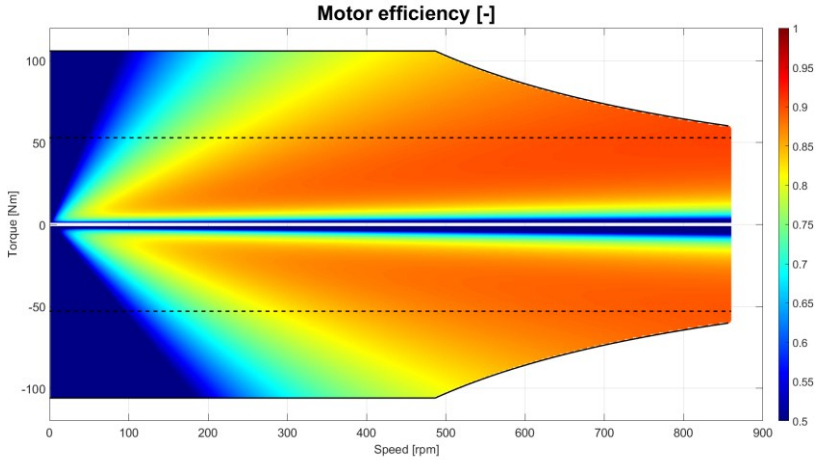

Fig. VI-6. Motor efficiency – analytical calculation

VI.2. Efficiency maps realization by simulation and data treatment

The MATLAB-Simulink model from Fig. IV-5 is used to investigate the capabilities of the motor. Depending on the rapidity of the computer and the available delay, pairs of speed-reference current requested to the motor are introduced into the simulation. Fig. VI-7 presents the process diagram for the operation.

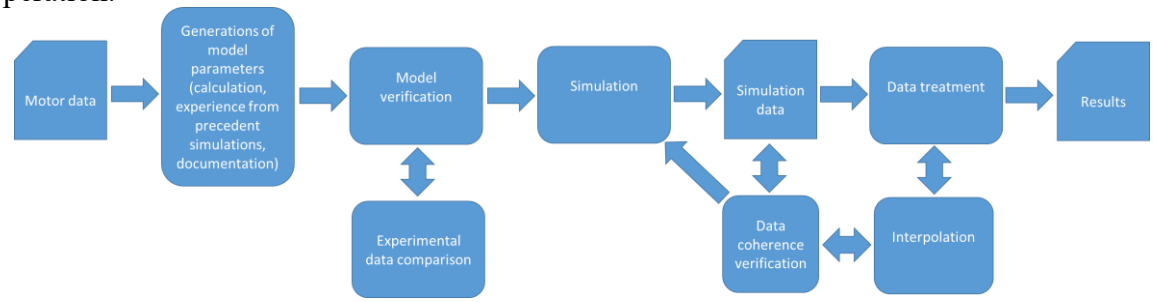

Fig. VI-7. Process diagram for efficiency maps data generation by simulation and data treatment

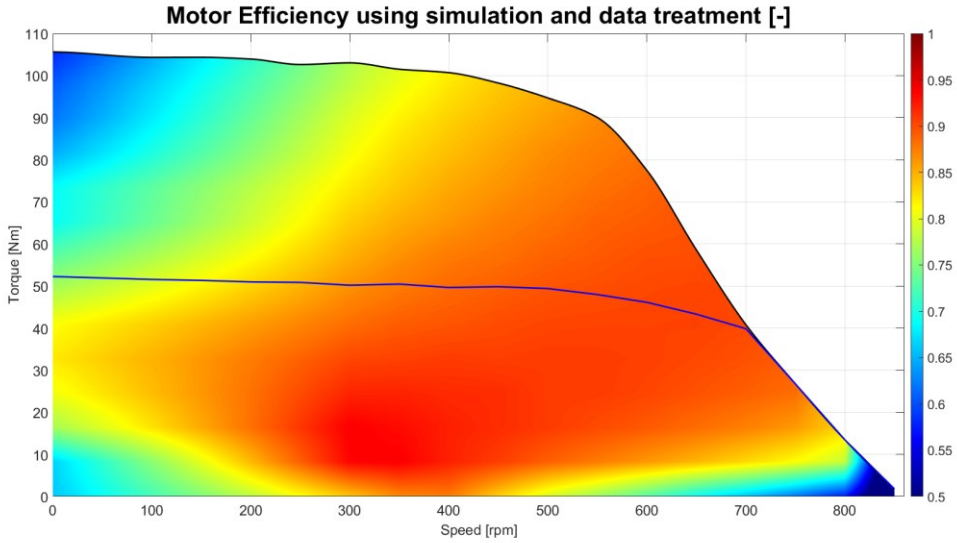

Fig. VI-8. Motor efficiency by simulation and data treatment

As the simulation integrates the dynamic regimes and transition phases of the physical entities during measurements, the physical entities need a supervision period depending on the dynamism of the transitions. Compared to the efficiency maps obtained by analytical calculation, the result in Fig. VI-8 becomes more natural and more realistic.

VI.3. Example of a powertrain constitution using previously obtained data

A vehicle based on Table V-4 and Table V-5 information is considered with two major modifications: the mass of the vehicle is increased to 400 Kg, and the wheel radius becomes 0.3 m.

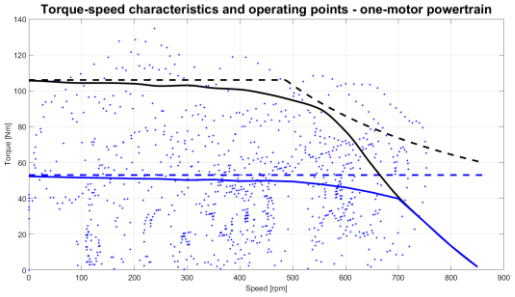

Fig. VI-9. Torque speed characteristic and operating points with one motor powertrain

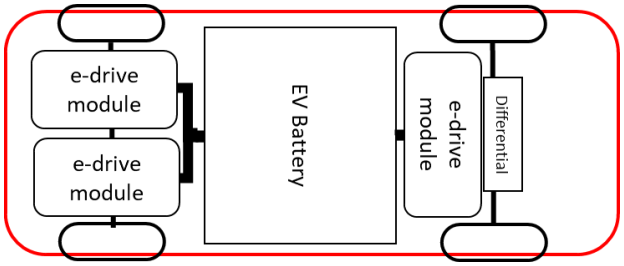

Fig. VI-10. New vehicle configuration with three motors

From the efficiency maps obtained previously by simulation and data treatment, three identical motors would be needed to cover the torque request in the high-speed region (between 1000s and 1500s of the WLTC). The investigation will consist of covering two cases of static load allocation: percentual load distribution of 40% on the frontal axle and 60% on rear axle (one motor will need to cover 40% of the requested torque and each of two other motors 30%), and optimal load distribution (in the case of identical motors, each motor must cover the torque request divided by the number of motors, 1/3 in this case). The energy efficiency results are synthesized in next two tables

Table VI-1. Energy efficiency for entire WLTC

Load distribution coefficient [%]	**Motor efficiency [%]**	**Total efficiency of the powertrain [%]**
30 %	80.2419	**80.9109464**

40%	81.9357	
Optimal load	81.0003	**81.0003**

Table VI-2. Energy efficiency for high-speed WLTC

Load distribution coefficient [%]	**Motor efficiency [%]**	**Total efficiency of the powertrain [%]**
30 %	82.4279	**83.2344458**
40 %	84.4743	
Optimal load	83.2976	**83.2976**

VI.4. Conclusions

To sustain the choice of multiple motors for an EV powertrain, the actual research has given a new methodology to realize the efficiency maps for a given PM BLDC motor. Based on the efficiency maps previously determined a three-motor powertrain has been investigated for energy efficiency. **The static load allocation with a percentual distribution of the total torque request by 60 % on rear axle with two identical motors and 40 % on frontal axle with a single motor, provides good results compared to the optimal load allocation between motors. The difference on the efficiency results is less than 0.09% for the entire testing cycle and less than 0.07 % only for high-speed.**

VII. Experimental Developments Preparation

VII.1.1. PMSM investigations

Fig. VII-1 shows the MATLAB-Simulink model used for PM motors when applying a sinusoidal control for the determinations.

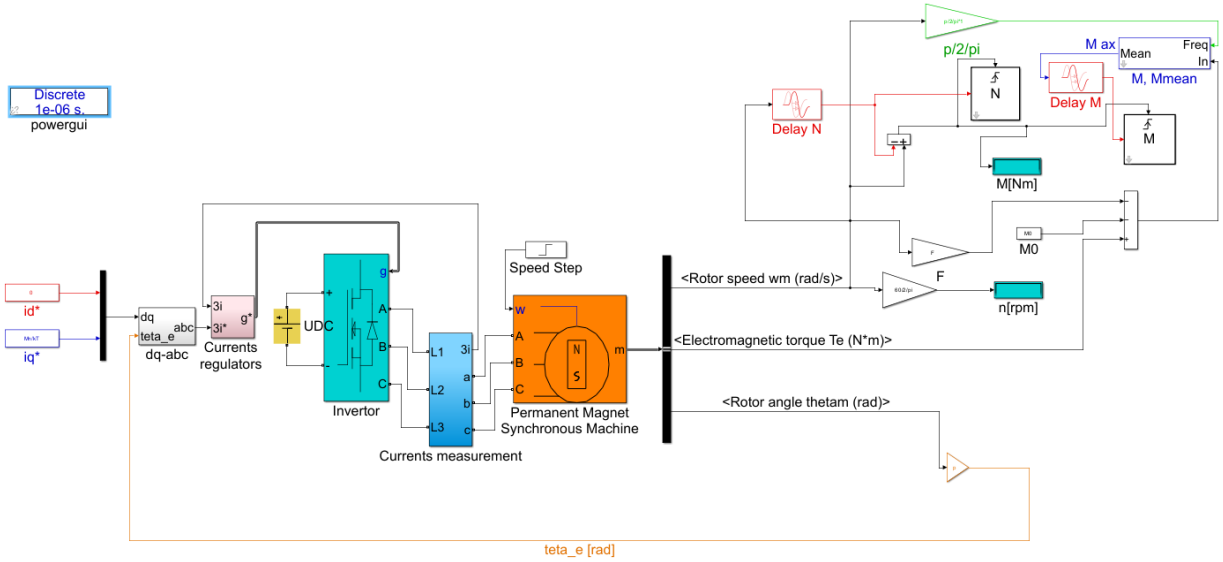

Fig. VII-1. Simulink model developped for PMSM investigations

VII.2. Preparations for physical platforms

VII.2.1. Electric sources

Fig. VII-2 presents a schematical view of the DC sources implemented for physical platforms.

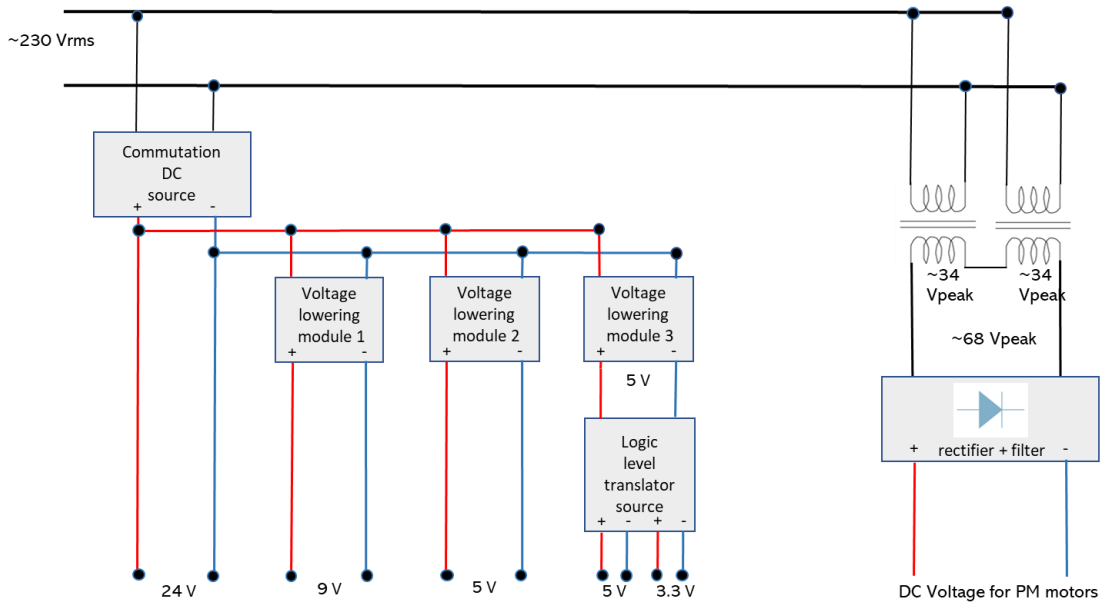

Fig. VII-2. Multiple DC voltage supply for platforms

VII.3. Resistant torque production

To produce a resistant torque during motors investigations a DC electric generator has been investigated and integrated into one of the physical platforms. Before any use of the generator, it has been checked from mechanical and electrical points of view.

Fig. VII-3. DC generator after refurbishment and integration on the physical platform

The next curve family has been determined regarding the possible resistant torque.

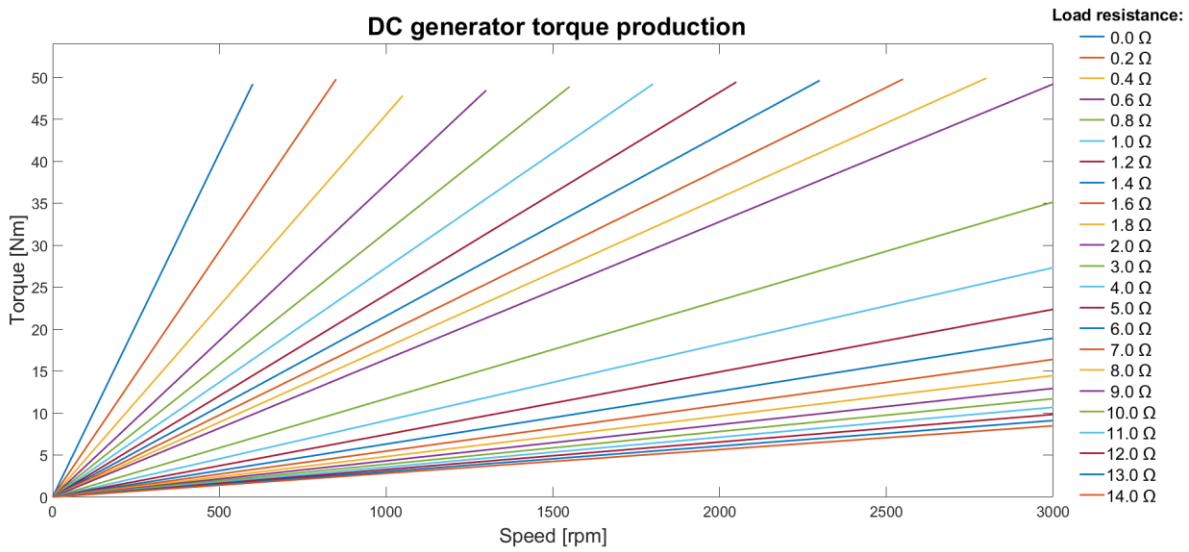

Fig. VII-4. Resistant torque produced by the DC generator

VII.4. Conclusion

As in precedent research, the simulation has been used before any physical test. A power supply system has been conceived to offer DC of 3.3, 5, 9 and 24 V for electronic control and measurement systems. A classic transformer followed by a rectifier and a filter was used to provide the voltage supply to PM motors. Developing and running the correspondent MATLAB-Simulink model, the parameters for the rectifier and filter have been determined. The physical results confirmed the simulated ones. For future developments a DC Switching Power Supply will be added. For creating resistant forces, like a real vehicle, a DC generator has been observed to be integrated on one of the physical platforms. A set of curves have been obtained giving the resistant torque production.

VIII. DEVELOPMENT OF PHYSICAL PLATFORMS AND MEASUREMENTS

VIII.1. Development of physical platforms

VIII.1.1. One independent motor

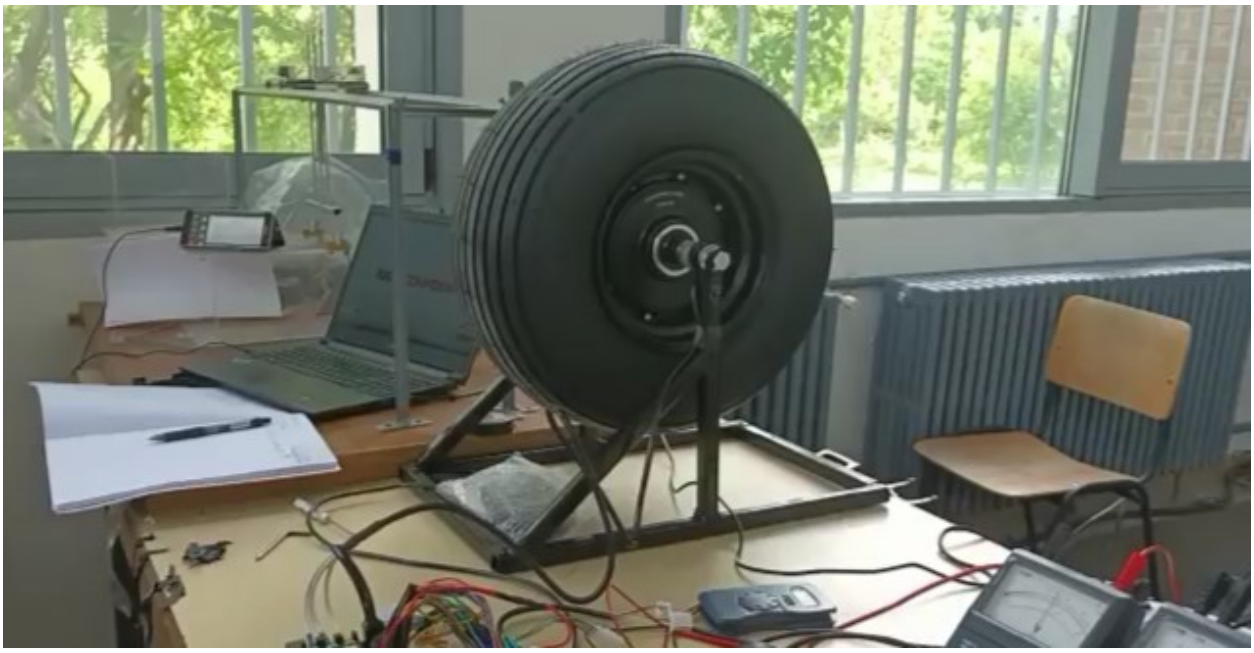

Fig. VIII-1. Physical platform integrating one single motor

VIII.1.2. Two motors running at same speed

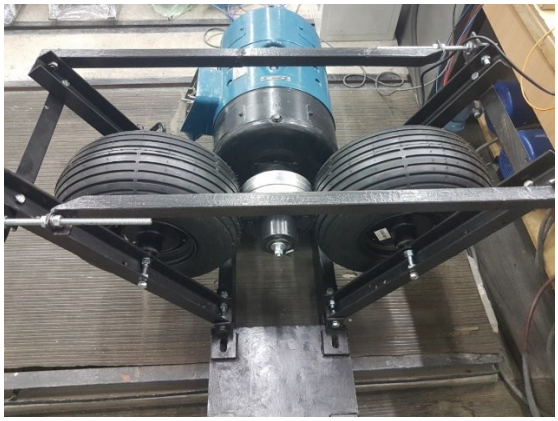

Fig. VIII-2. Platform with two in-wheel motors – image on coupling between wheels

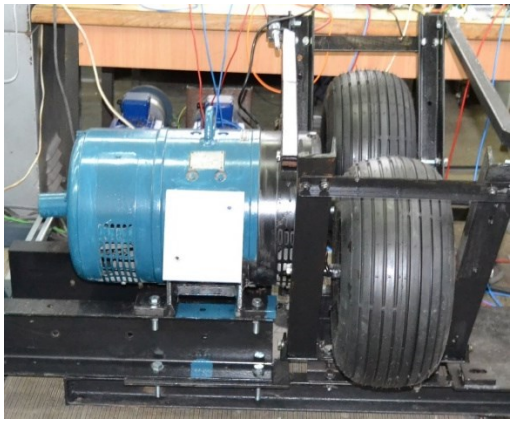

Fig. VIII-3. Platform with two in-wheel coupled motors – final stage

VIII.1.3. Two independent motors

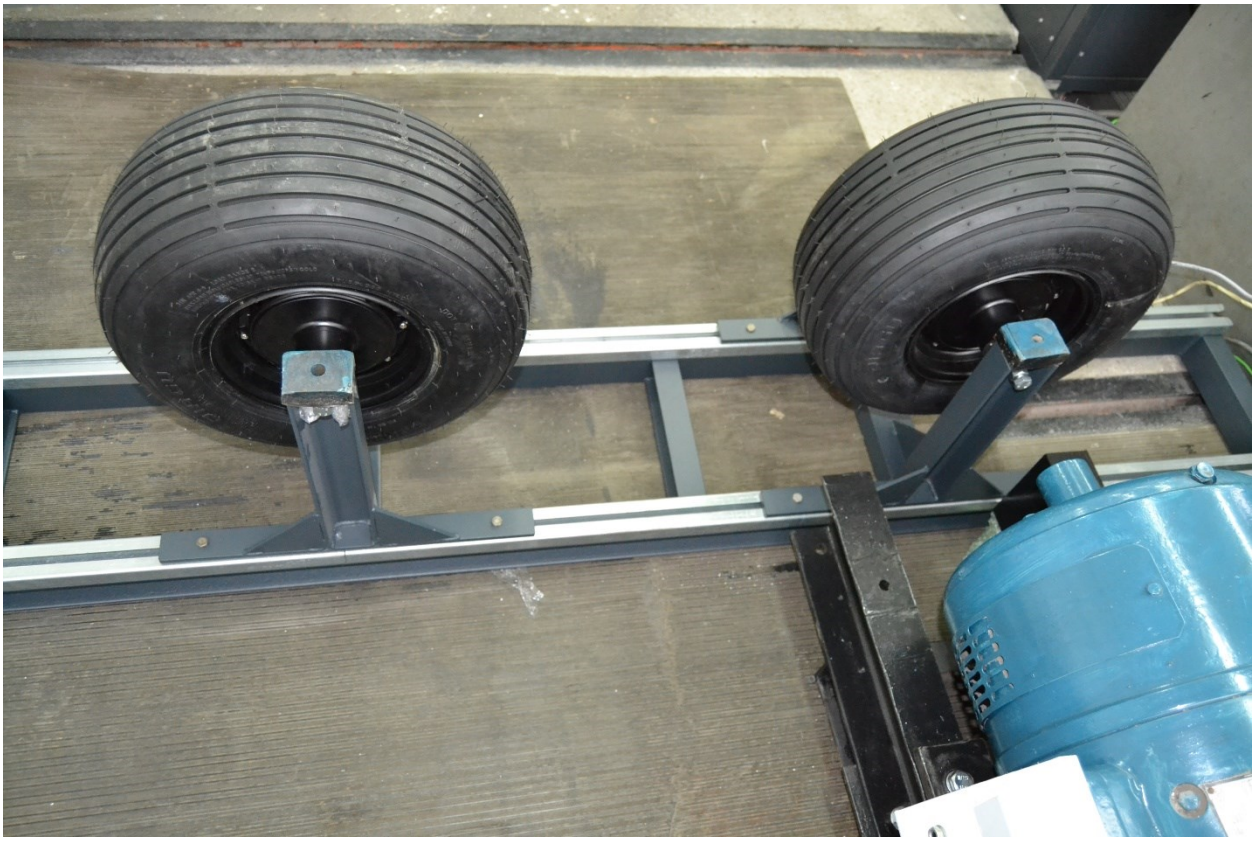

Fig. VIII-4. Platform with two independent in-wheel motors – the final stage

VIII.1.4. Platforms control implemented with STM32 microcontroller

There was a need to integrate a microcontroller with enough I/O possibilities to supervise at least two motors on a single platform.

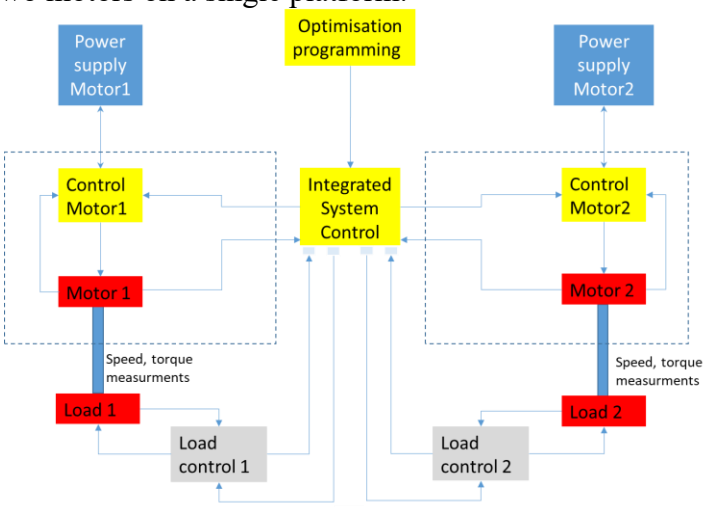

Fig. VIII-5. General view on the platforms management system

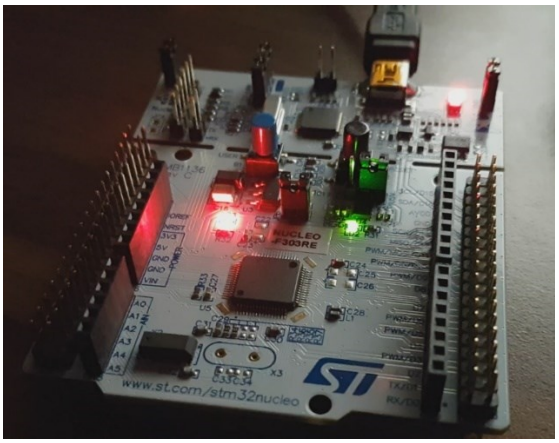

Fig. VIII-6. Microcontroller STM32 F303RE

<u>Speed profile implementation, Speed measurement, Speed Control</u>

The research on PM motors explained previously was regularly conducted to an application on standardized testing cycle, WLTC or FTP75.

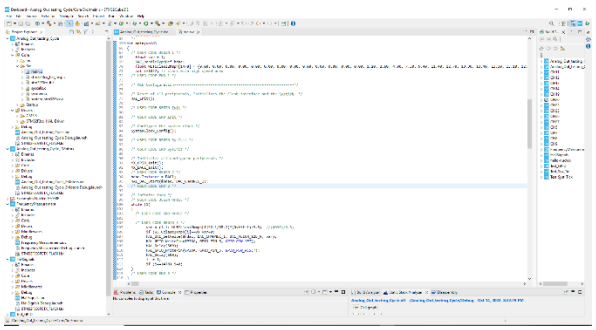

Fig. VIII-7. Main routine for WLTC speed profile request

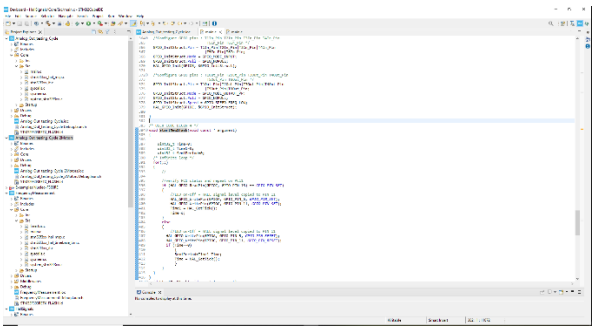

Fig. VIII-8. Routine for measuring the Hall signal period

VIII.2. Physical determinations

VIII.2.1. Measurements

Fig. VIII-9. Running the PM motor as a generator for firsts determinations

Fig. VIII-10. PM motor – phase-to-phase resistance and inductances measurement

VIII.2.2. Constitution of the DC Electro-Mechanical Convertor (DCEMC)

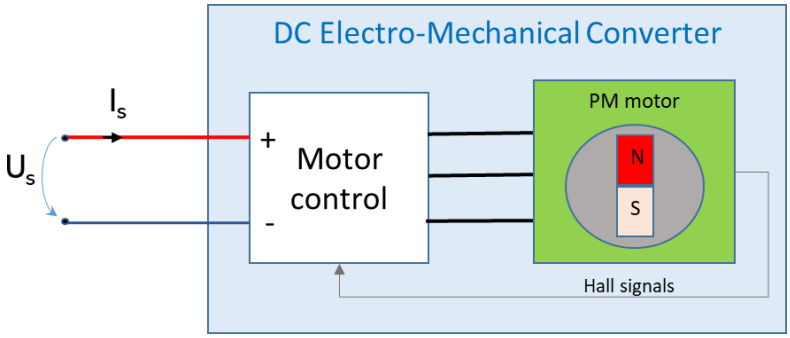

Fig. VIII-11. Seeing the motor control and the PM motor as a DCEMC

VIII.2.3. Determination of the operational area of the motors

The next determinations refer to the acquired PM motors installed on the platforms described previously. Combining simulation, following the model presented in Fig. VII-1, and physical measurements, it was possible to obtain more accurate results.

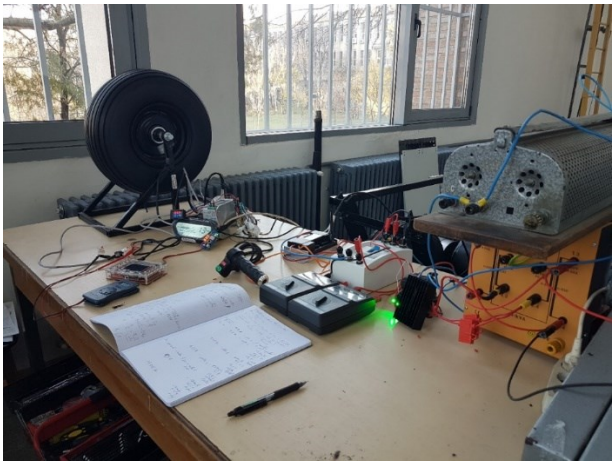

Fig. VIII-12. Physical measurements – general view on no-load situation

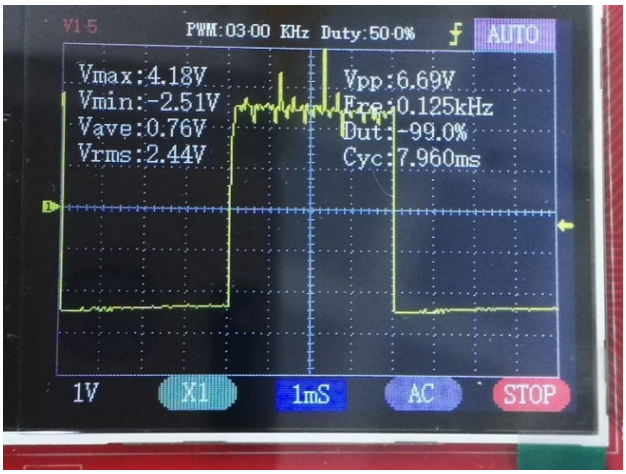

Fig. VIII-13. Hall signal on the scope for a vehicle speed of 32 km/h

The speed measured on onboard device gave an indicative value. The more precise value has been calculated based on measurement on Hall signals period. The determination of the lost power coefficients, T_{f0} and F_v, supposed several measurements in no-load and load conditions at different speeds. Consistency between results was sought when selecting appropriate values. The two coefficients have resulted from the retained values: T_{f0}=0.986 Nm and F_v=0.005 Nms. From the commercial data of the acquired motors, there is a theoretical maximum speed $v_{n_{\max}} = 50$ km/h, without running time limit, accepted by the vehicle having a propulsion system with a single motor, for a nominal voltage of 60 V. It means that the motor can run continuously at the correspondent angular speed and the internal developed heat can continuously be evacuated. The second information available was the maximum power of $P_{out_{\max}} = 1500$ W. The motor can deliver this power during a limited period of time (seconds). For the wheel radius $r_w = 0.225$ m, without any gear ratio between wheel and motor (in-wheel motor) it results the maximum rated angular speed, 61.37 rad/s. It represents a theoretical maximum speed of 589.78 rpm. For the platform in Fig. VIII-2, where the transmission ratio between the electric motor and the generator is 1:2.3, for the DC generator rotor results a speed of 1356.5 rot/min. For a vehicle having the mass $M_{veh} = 200$ kg, moving on concrete with a rolling resistance coefficient $c_r = 0.013$, with a vehicle frontal area $S_{veh} = 0.95$ m^2, and a vehicle aerodynamic drag coefficient $c_x = 0.46$, it results the total resistant force $F_{total} = 77.138$ N and corresponding to a torque $T_{n_{\max}} = 17.356$ Nm. **There is the confirmation that the physical platform with two coupled motors can provide via the DC generator enough resistant torque for both motors.** The maximum output power of 1500 W at the maximum speed of 50 km/h, corresponds to a peak torque of 24.3 Nm. Running the motor in no-load generator mode and measuring the terminals voltage it results the back-EMF constant $k_E =$ 1.14 V_{peak}·s/rad. The obtained torque constant is $k_T =$ 0.99 Nm/A_{peak}. Neglecting the losses it results the values for the maximum rms values for the current passing through the motor for maximum nominal speed (with no time limit) and for maximum power (limited time), 12.34 A and respectively 17.28 A. **There is the confirmation that the physical platform with two coupled motors can be supplied with electric energy from DC source specially developed for the motors**. The previously obtained data are processed under MATLAB to generate a graphical representation in the next figure.

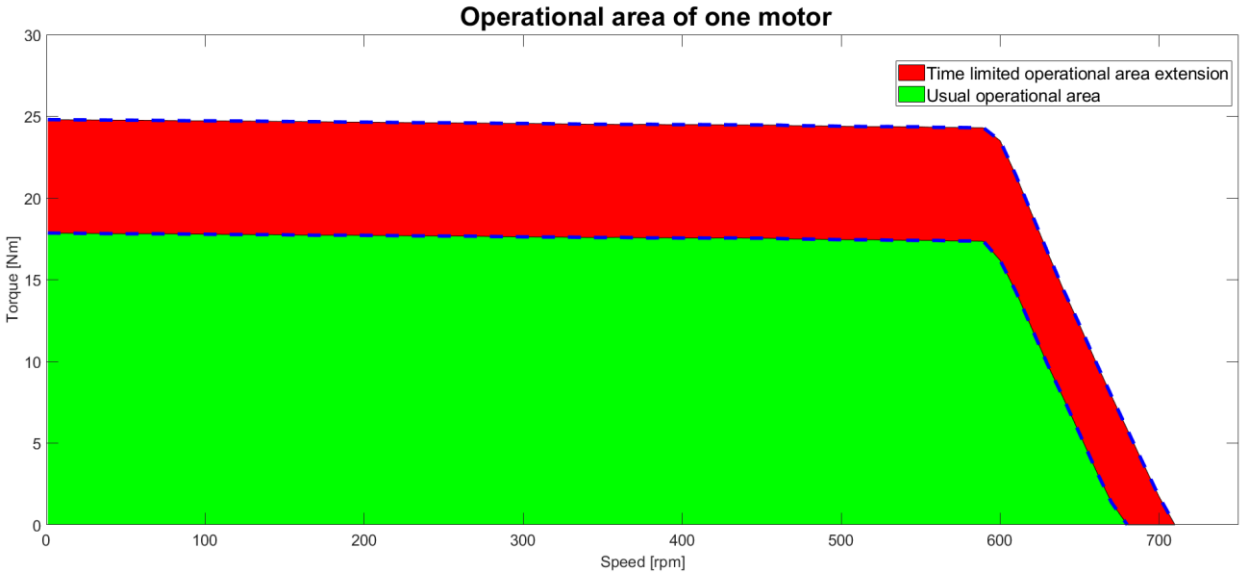

Fig. VIII-14. Operational area of the investigated motor

VIII.3. Conclusions

The actual work emphasized the complementary information needed, and activities to make possible the research and to help in the confirmation of the results. The conception of physical platforms, complementary voltage sources, measurement tools, and dedicated control devices are examples of time-consuming activities. There is satisfaction when all of them come to support the research. On the other hand, the complementary obtained knowledge offers perspectives for future studies and developments. The DCEMC example is conclusive as the onboard stored electric energy in the electric battery directly offers a DC voltage source. There is a need to transform and adapt it for better performance. Nowadays, simulation tools attempting a certain level of confidence are more and more used to obtain an image of a future reality. However, there is a need for fine tuning of the simulation parameters to obtain more realistic results. The operational area of motors has been built based on available information on the motors, simulation, and physical measurements.

IX. General Conclusions and Further Research Opportunities

Energy consumption optimization strategy, being a complex and a multidomain subject, the beginning of the research was concentrated on building step by step their main objective. Additional sub-objectives have been established on the road to the main one.

In chapter II, the preparation phases related to simulation implementations are presented. The main components of the vehicle simulation represent the first results of this work. Afterwards, the transformation of the normalized speed request in tractive effort to be developed by the powertrain is realized starting from main vehicle and road characteristics. The methodology to obtain the correspondent operating points is built and explained. Two different BLDC motors are used to continue the research by building and implementing the process for the operational area study by analytic calculation using programming and obtaining the motor characteristics. Finally, the coverage of the operating points by each motor is analyzed.

Chapter III builds specific static, dynamic, and mixed load allocations methods. Inside each method, load distribution criteria are defined and analyzed, following the efficiency impact when applied: complementary, percentual, proportional and optimal distributions for the static method, load

distributions based on past and future situations and internal losses minimization distribution for dynamic method, and extension of vehicle capabilities using the mixed method. The method and the calculation for the iron losses coefficients depending on motor speed and square motor speed is presented. During the entire testing cycle the studied powertrain with a single motor consumes about 10% more energy than the powertrain with two motors in a complementary load allocation. Also, the application of the complementary load allocation starting with one motor, or the other, is not without importance. It had an additional positive impact in energy consumption (about 1%). Regarding the load distributions using a fixed percentage, the proportional load allocation gives satisfaction as the motors are charged proportionally with their capabilities, and there is no risk to overcharge a motor. The optimal load distribution is obtained from the analytical model, searching to maximize the powertrain efficiency. In the assumptions of the method, it was obtained the optimal load distribution coefficient for each motor of the powertrain as a constant value during the operational area coverage. The process for motor and powertrain efficiency maps determination by analytic calculation are then built and presented. Comparing the resulting efficiency maps, the optimal load distribution generated the best efficiency of the powertrain. Continuing load allocation methods investigation, the dynamic one was defined by a load distribution specific calculation in each operating point. The results on internal losses minimization for each operating point are compared with a static load distribution between motors. Improvements of 0.2 % on a flat surface and 3.4 % for a slope of 15 degrees, are generated in comparison to the percentual load allocation of 40%-60% for the bi-motor powertrain. The mixed load distribution method is used to emphasize the difference between optimal load distribution (with the extension by dynamic load allocation) and the case of the powertrain with a single motor. An extension of the vehicle usage has been studied up to the superior limits of the electric motors. Chapter III ends by presenting a new method to explore the vehicle capabilities starting from the powertrain characteristics.

Advanced methods to improve motor characteristics and vehicle performance have been studied using BLDC propulsion system in chapter IV. The motor simulated model allows to introduce two methods for improving motor characteristics: phase advance and dwell control methods. The simulation is used to obtain the motor characteristics. A dedicated model has been developed using the motors parameters, a dedicated speed profile for operational area investigations, calculating the vehicle resistant forces, and, finally, providing the operating points. A specific implementation schema is developed and presented for phase advance and dwell control methods. The mathematical model for phase advance and dwell control angles is built. It generates a specific model developed under simulation.

Once the simulation is implemented, chapter V is dedicated to performing the investigations and providing the results. The entire operational area for the vehicle simulated in chapter IV has been investigated. Regarding the powertrain, its operational area is built by a new method using simulation for nominal and respective maximum current supported by the motors, and for phase advance angles from 0 to 60 degrees (considered as the extreme). The operational area of the motor can be enlarged using phase advance for high speeds, and the no-load speed obtained is 2662.85 rpm (more than three times the maximum speed of the motor without phase advance). The applied method confirms an improvement in a motor current at high speeds when using phase advance, in parallel with an increase in the torque ripples. In addition, the dwell control method was applied in parallel with phase advance. The obtained improvement consists in reducing the torque ripples, reducing the torque reduction at low speeds, and growing the torque at high speeds (around the no load speed obtained without applying phase advance and dwell control methods). The increase of the dwell control angle impacts the shape of the current more, moving it to a sinusoidal one. Approaching the maximum no load speed attempted using phase advance, as the shape of the current is more and more sinusoidal, the effect of dwell control angle reduces. The method to generate the dependence of the powertrain torque on phase advance and dwell control angles had been presented with examples of 3D representations.

Finally, a complement to the simulation model is added to obtain the respective angle pairs, increasing the powertrain efficiency in each operating point. An additional model has been developed to measure the impact on energy consumption. For the investigated vehicle, the application of the method has given reduction of about 18% in the energy consumption during WLTC. As a general conclusion, using phase advance and dwell control, the BLDC powertrain, for a given vehicle is able to perform better in terms of torque production, speed, and efficiency.

New methodologies to realize the efficiency maps of the motors and to choose the number of motors in an EV powertrain are developed in Chapter VI. For a vehicle with three identical BLDC motors, the optimal load distribution gives the best results, but the static load allocation with a percentual distribution of the total torque request by 60 % on rear axle with two identical motors and 40 % on frontal axle with a single motor, provides good results too. The difference on the efficiency results is less than 0.09% for the entire testing cycle and less than 0.07 % only for high-speed region.

For physical experiments and measurement (chapter VII), it was a necessity to build a power supply for controlling the testing platforms and measuring the physical entities. Additional power supply for PM motors have been developed using simulation before choosing the physical components. For the resistant torque production, a DC generator had been measured and investigated realizing the torque curves dependence on speed and generator load. Chapter VIII continuous the experiments preparation completing the physical aspects by the development of three physical platforms for PM motors: one independent motor, two motors running at same speed coupled on load, and two independent motors. For the investigations the platforms supervision is realized by a STM32 microcontroller with specific programs released for speed profile implementation, speed measurement and speed control. There is also the introduction to a new concept: the DCEMC – DC Electro-Mechanical Convertor. Using physical measurements, the operational area of the acquired motors for the platform are obtained.

The processes, methods, and physical platforms developed and presented previously opens ways for further research based on PM motors, combining the load allocation methods (chapter III, chapter VI), individual motors improvements (chapter IV, chapter V), in the realization of multi-motor powertrains (chapter II, chapter VI). The physical platforms help the confirmation of the simulation parameters. They support future developments related to multi-motor powertrains, as specific torque and speed control for motors powering individually a vehicle wheel, under the constraint of vehicle stability, when searching energetic improvements.

ORIGINAL CONTRIBUTIONS

The research has been conducted using Permanent Magnets (PM) motors by software programming calculation, development of models and simulation, and experimental data verification on dedicated developed platforms. The main achievements are listed below.

1. Reduction in electric energy consumption for an Electric Vehicle (EV) using multi-motor powertrains:

- research regarding the usage of two smaller motors instead of one bigger equivalent motor generating energy optimization,
- realization of different strategies for load allocation between the motors of the powertrain (static, dynamic, and mixed load allocations strategies),
- studies regarding the impact of load allocations on the resulting efficiency maps of the powertrain,
- investigations on static load allocations: complementary, percentual, proportional, and optimal load distributions and methodology to calculate an optimal load distribution starting from motor characteristics,
- investigations on motor internal losses minimization,
- study of a powertrain with two identical motor types but with different characteristics for operational area extension using mixed load allocation,
- construction of the curve limits for a given powertrain depending on mass and slope angle.

2. Application of Phase Advance (PA) and Dwell Control (DC) methods for:

- increasing the maximum speed of the propulsion system,
- maximizing the torque produced by the powertrain,
- optimizing the powertrain efficiency,
- generating the influence of PA and DC angles on powertrain precedent characteristics.
- maximizing the motor yield,
- reducing the energy consumption of the EV using the respective powertrain,

3. Methodology elaboration for building efficiency maps of motors:

- a methodology based on analytic calculation, simulation, and data treatment,
- application of the result in the constitution of multi-motor powertrains (three motors)
- impact analysis on energy efficiency for approaching the results of optimal load distribution by vehicle configuration and percentual load distribution

4. Multi-motor experimental platforms realization:

- physical investigations on PM in-wheel motors,
- physical investigations using independent motors,
- physical investigations using motors running at the same speed,
- implementation of a controlling and monitoring system,
- installation of additional required equipment.

PUBLICATIONS OF THE AUTHOR

I. Books

Ca1. C.L. Popescu, N. Vasiliu, M. Ivănescu, *Cercetarea și dezvoltarea de sisteme și soluții pentru mobilitate durabilă*, Ed. Politehnica Press, Bucuresti, 104 p. ISBN 978-606-515-633-3 2015

II. Published articles / extended studies in Journals

Ris ISI journals / BDI indexed journals / International Journals

Ris1. L. Popescu, L. Melcescu, L. Dumitran, A. Crăciunescu, A. Stănescu, "Control Analysis of a Bi-motor Electric Traction System for Energy and Performance Optimization", accepted for AIP Conference Proceedings at *International Conference on Communications, Information, Electronic and Energy Systems - CIEES 2021,* November 25 – 27, 2021, AIP Conference Proceedings 2570, 040002 (2022); https://doi.org/10.1063/5.0099663 Published Online: 18 August 2022
Index: The Conference Proceedings Citation Index (part of Web of Science), Scopus (Elsevier), Inspec, Chemical Abstracts Service (CAS), Astrophysics Data System (ADS)).
Index: SCOPUS AUTH. ID:57238783500

Ris2. C.L. Popescu, L. Dumitran, A. Stănescu " Simulation of Multi-Motor Propulsion System for Energy Efficiency in Electric Vehicles" in *Annals of the University of Craiova, Electrical Engineering series,* No. 45, Issue 1, 2021, published the 21st of January 2022; pp 75-82; ISSN 1842-4805, ISSN 1842-4805, DOI: 10.52846/AUCEE.2021.1.11
https://elth.ucv.ro/fisiere/anale/wp-content/uploads/2022/01/11-2021.pdf,
https://doi.org/10.52846/aucee.2021.1.11, Index: Copernicus, Cat. B+ Journal CNCSIS

Ris3. O. Craiu, I. Ichim, **L. Popescu**, " FEM Study of a Brushless Synchronous Motor with different Permanent Magnet Topologies, 2022 - Scientific Bulletin of University Politehnica of Bucharest, Series C Electrical Engineering and Computer Science, ISSN 2286-3540
https://www.scientificbulletin.upb.ro/rev_docs_arhiva/reze02_229821.pdf
Index; ISI Thomson Reuters, INSPEC, SCOPUS, ELSEVIER SCIENCES BIBLIOGRAPHIC DATABASES, Metadex, ENGINEERING VILLAGE, CAMBRIDGE SCIENTIFIC ABSTRACTS, ENGINEERED MATERIALAS ABSTRACTS, Cat. B+ Journal CNCSIS, Web of Science Core Collection: Emerging Sources Citation Index, Index: SCOPUS AUTH. ID:57238783500

Ris4. C.L. Popescu, "RTR's involvement in continuous improvement of quality and reliability of Renault Group's vehicles", in *Fuel Economy, Safety and Reliability of Motor Vehicles (ESFA 2009)*, Bucharest, Romania, 2009, Publisher SIAR,
https://go.fisita.com/store/papers/ESFA09/E09C104

Rns. National Journals, CNCSIS

Rns1. L. POPESCU, A. Stănescu, "Efficiency maps for an EV BLDC motor using analytic calculation and simulation", *in Electric machines, materials and drives present and trends* (SME 2022), APME, vol. 18, nr. 1, pp. 89-99, March. 2023, retrieved from https://journal.iem.pub.ro/apme/article/view/352, ISSN / ISSN-L: 1843-5912

Rns2. L. Popescu, A. Stănescu, Șt. Vasiliu, "Didactical platform for multi-motor solutions", in *Electric machines, materials and drives present and trends* (SME 2021), APME, vol. 17, nr. 1, pp. 172–181, ian. 2022, retrieved from https://journal.iem.pub.ro/apme/article/view/131
ISSN / ISSN-L: 1843-5912, https://www.doi.org/10.36801/apme.2021.1.17

Rns3. L. Popescu, "Electromobility topics entering a new decade", in *Electric machines, materials and drives present and trends* (SME 2020), APME, vol. 16, nr. 1, pp. 131–140, ian. 2021, retrieved from https://journal.iem.pub.ro/apme/article/view/209, ISSN / ISSN-L: 1843-5912, https://www.doi.org/10.36801/apme.2020.1.13

Rns4. C.L. Popescu "RTR's involvement in continuous improvement of quality and reliability of Renault Group's vehicles" in *Ingineria Automobilului*, nb. 14 , pp. 4-8, / March 2010, ISSN 1842 – 4074, http://siar.ro/wp-content/uploads/2014/02/RIA_14.pdf

Index: Web of Science - Emerging Source Citation Index (ESCI)

III. Conferences - published articles / extended studies / conference proceedings

Vis. International conferences

Vis.1 L. Popescu, O. Craiu and L. Melcescu, "Analyzing the Torque Transfer between Two In-Wheel Motors of an Electric Vehicle," *2023 13th International Symposium on Advanced Topics in Electrical Engineering (ATEE)*, Bucharest, Romania, 2023, pp. 1-6, doi: 10.1109/ATEE58038.2023.10108365.
Index: IEEE Xplore, Clarivate (WOS) and SCOPUS listed conferences
https://ieeexplore.ieee.org/document/10108365
WOS: ongoing, Index: SCOPUS ongoing

Vis.2 O. Craiu, T. -I. Ichim and **L. C. Popescu**, "3D FEM Model of a Hybrid Stepper Using Scalar-Vector Potential Formulations," *2023 13th International Symposium on Advanced Topics in Electrical Engineering (ATEE)*, Bucharest, Romania, 2023, pp. 1-5, doi: 10.1109/ATEE58038.2023.10108283.
Index: IEEE Xplore, Clarivate (WOS) and SCOPUS listed conferences, https://ieeexplore.ieee.org/document/10108283, WOS: ongoing, Index: SCOPUS ongoing

Vis.3 L. Popescu, L. Melcescu and O. Craiu, "Energy Efficiency Improvement for an Electric Vehicle PM BLDC Propulsion System Using Phase Advance and Dwell Control," *2022 International Conference on Electrical, Computer, Communications and Mechatronics Engineering (ICECCME)*, 2022, pp. 1-6, doi: 10.1109/ICECCME55909.2022.9988388.
https://ieeexplore.ieee.org/document/9988388, INSPEC: 22474858, Index: SCOPUS AUTH. ID:57238783500

Vis.4 L. Popescu, L. Melcescu, O. Craiu, A. Craciunescu and V. Bostan, "Phase Advance and Dwell Control Applied to a PM BLDC Motor for Increasing the Maximum Speed of an Electric Vehicle," *2022 International Symposium on Power Electronics, Electrical Drives, Automation and Motion (SPEEDAM)*, 2022, pp. 850-855, doi: 10.1109/SPEEDAM53979.2022.9841974.
https://ieeexplore.ieee.org/document/9841974, INSPEC: 21930188, Index: SCOPUS AUTH. ID:57238783500

Vis.5 O. Craiu, T. I. Ichim, L. M. Melcescu and **L. Popescu**, "Optimization of a High Torque Density Small Hybrid Stepper using 3D FEM Model," *2022 International Symposium on Power Electronics, Electrical Drives, Automation and Motion (SPEEDAM)*, 2022, pp. 610-615, doi: 10.1109/SPEEDAM53979.2022.9842105.
INSPEC: 21930247, https://ieeexplore.ieee.org/document/9842105, Index: SCOPUS AUTH. ID:57238783500

Vis.6 L. Popescu, L. Melcescu, L. Dumitran, A. Crăciunescu, A. Stănescu, "Control Analysis of a Bi-motor Electric Traction System for Energy and Performance Optimization", accepted for AIP Conference Proceedings at *International Conference on Communications, Information, Electronic and Energy Systems - CIEES 2021,* November 25 – 27, 2021
https://www.youtube.com/watch?v=wSWsFHot9nU&list=PLFXbUXJmS8n_xzwDQQD0wBaqJTk8YWeF9&index=3

Vis7. L. Popescu, L. Melcescu, L. Dumitran, and A. Crăciunescu, " Analysis of the influence of wheel torque distribution on energy efficiency in the case of an electric vehicle with two motors" [abstract], in Proceeding book of 1st Internatıonal Conference on Applıed Engıneerıng and Natural Scıences (ICAENS), 1-3 November 2021, Konya, Turkey pp. 300
https://drive.google.com/file/d/1ZYtf6Db1lJezKksVtqHqBKID-Mv9BtxU/view?usp=sharing

Vis8. L. Popescu, L. Dumitran and A. Stanescu, "Multi-motor solutions for electric vehicles," *2021 International Conference on Applied and Theoretical Electricity (ICATE)*, 2021, pp. 1-6, doi: 10.1109/ICATE49685.2021.9465016,
IMSPEC: 20895693, WOS:000709089900039, Index: SCOPUS AUTH. ID:57238783500

Vis9. Marinescu D.G., Nicolae V., **Popescu C.L**., Calin L., Mierloiu N., Andreescu C., Clenci A. (eds) (2016) DUSTER ZERO—Electric Vehicle Research 4WD. In: Proceedings of the European Automotive Congress EAEC-ESFA 2015. Springer, Cham. https://doi.org/10.1007/978-3-319-27276-4_4

Vis10. Marinescu, D., **C.L. Popescu**, Ion Tabacu, V. Nicolae, Florin Serban, Ș. Tabacu, I. Vieru and Iorga Adrian. "EVS 28 KINTEX , Korea , May 3-6 , 2015 A Full Electric Vehicle 4 WD Type." (2015)

Index: SCOPUS AUTH. ID:57238783500

Vis11. C.L. Popescu, "RTR's involvement in continuous improvement of quality and reliability of Renault Group's vehicles", Presented at: Fuel Economy, Safety and Reliability of Motor Vehicles (ESFA 2009), November 2009, organized by SIAR, Bucharest, Romania

Vn. National conference volumes

Vn1. L. Popescu, A. Stănescu, " Efficiency maps for an EV BLDC motor using analytic calculation and simulation" in *Electric machines, materials and drives present and trends* symposium, XVIII edition (SME 2022), Bucharest, the 9th of December 2022, published in IEM journal

Vn2. L. Popescu, A. Stănescu, Șt. Vasiliu, "Didactical platform for multi-motor solutions", in *Electric machines, materials and drives present and trends* symposium, XVII edition (SME 2021), Bucharest, 19th of November 2021, published in IEM journal

Vn3. L. Popescu, "Electromobility topics entering a new decade", in *Electric machines, materials and drives present and trends* symposium, XVI edition (SME 2020), Bucharest, 20th of November 2020, published in IEM journal

IV. Articles accepted / sent for future publication – International Journals / Conferences

Ris4. L. Popescu, O. Craiu, "Energy Consumption Analysis for an EV Powertrain using Three BLDC Identical Motors", for Rev. Roum. Sci. Techn.– Électrotechn. et Énerg Vol. xx, y, pp. uuu–zzz, Bucarest, 2023.

Index Clarivate Analytics (ex Thomson Reuters) JCR impact factor (2021/2022): 0.670, Web of Science Core Collection: Science Citation Index Expanded, Additional Web of Science Indexes: Essential Science Indicators, Revue Roumaine des Sciences Techniques, Série Électrotechnique et Énergétique is a journal of the Romanian Academy, the Engineering Section

Ris5. O. Craiu, I. Ichim, **L. Popescu**, " Analyzing a Three-Hundred Teeth bi-phase Hybrid Stepper Motor with different Numbers of Pole-pairs ", for Rev. Roum. Sci. Techn.– Électrotechn. et Énerg Vol. xx, y, pp. uuu–zzz, Bucarest, 2023.

Index Clarivate Analytics (ex Thomson Reuters) JCR impact factor (2021/2022): 0.670, Web of Science Core Collection: Science Citation Index Expanded, Additional Web of Science Indexes: Essential Science Indicators. Revue Roumaine des Sciences Techniques, Série Électrotechnique et Énergétique is a journal of the Romanian Academy, the Engineering Section

Vis12. L. Popescu, A. Crăciunescu, O. Craiu, " Analysis of the Wheel Steering Influence on Energy Consumption of an EV PMSM In-wheel Propulsion System", for *Interdisciplinarity in Engineering* (INTER-ENG 2023, the 16th edition)

The Proceedings of the 15th edition of the International Conference on Interdisciplinarity in Engineering has been indexed by Clarivate Analytics Conference Proceedings Citation Index-Science (CPCI-S) in Web of Science Core Collection (ISI Web of Science)